A STUDY ON ELECTRICAL DEGRADATION, PROCESSING AND INTERFACIAL STRENGTH OF CARBON FIBER EPOXY COMPOSITES WITH POLYMERS AND FILLERS

By

DEVIPRAKASH JYOTHISHMATHI

Bachelor of Technology in Mechanical Engineering
Kerala University
Trivandrum, India
2013

Master of Science in Mechanical Engineering
Khalifa University
Abu Dhabi, UAE
2017

Submitted to the Faculty of the
Graduate College of the
Oklahoma State University
in partial fulfillment of
the requirements for
the Degree of
MASTER OF SCIENCE
December, 2022

A STUDY ON ELECTRICAL DEGRADATION, PROCESSING
AND INTERFACIAL STRENGTH
OF CARBON FIBER EPOXY COMPOSITES
WITH POLYMERS AND FILLERS

Dissertation Approved:

Dr. Raman P. Singh

Dissertation Advisor

Dr. Ranji Vaidyanathan

Dr. Jake Bair

ACKNOWLEDGMENTS

Firstly, I am grateful to God for the blessings he has provided that allowed me to pursue this program and arranging such great individuals to guide and motivate me along the way.

I am very much thankful to my advisor, Dr.Raman P. Singh, for guiding me through the ups and downs of research and for driving me in the right direction. I am deeply indebted for this opportunity and the financial support you have given me in this course.

I take this opportunity to thank and remember my father and grandmother, who passed away, for all the support and love they showed to me. I would also like to thank my dear mother, brother and his family for all their affection and support. You have given me the best possible things in life and there is no repaying such a gift, thank you.

To my committee members, Dr. Ranji Vaidyanathan and Dr. Jake Bair, thank you for your guidance and suggestions on this research project.

I lovingly acknowledge my fellow lab mates Sai Tarun and Alan Austin for their continuous support and inputs. I would also like to thank graduate student Siddhesh Chaudhari for helping me with the DMA measurements.

To the rest of my family, thank you all for the support, I carry all of these with me.

Acknowledgments reflect the views of the author and are not endorsed by committee members or Oklahoma State University.

Name:	DEVIPRAKASH JYOTHISHMATHI
Date of Degree:	DECEMBER, 2022
Title of Study:	A STUDY ON ELECTRICAL DEGRADATION, PROCESSING AND INTERFACIAL STRENGTH OF CARBON FIBER EPOXY COMPOSITES WITH POLYMERS AND FILLERS
Major Field:	MECHANICAL AND AEROSPACE ENGINEERING

Abstract: The electric current induced damages in carbon fiber composites necessitates an improvement in their electric and thermal properties. The study investigates the effect of graphene as a filler material in carbon fiber epoxy composites with regards to their electrical, mechanical, and viscoelastic properties. Cross ply carbon fiber laminates with epoxy and epoxy loaded with three different concentrations of graphene (0.7, 1.4 and 2.8 wt.% of epoxy) are fabricated by hand layup technique. The specimens are subjected to a constant current density of 46 kA/m^2 for 3 hours and the variation in resistance and temperature are monitored real-time. Dynamic mechanical analysis (DMA), combined loading compression testing (CLC), three-point bend test, transverse and through thickness resistivity measurements are performed after electrical degradation. To differentiate the effect of thermal and electrothermal behavior, a few samples in each case are exposed to isothermal conditions. It is noticed that the addition of graphene led to a significant decrease in resistance (17-49 %) and temperature (17-39 %) of the specimen when electric current is passed through them. A 9-25 % increase in T_g along with a low variation of tan δ is observed for graphene loaded samples. A significant improvement in both compressive and flexural strengths are reported for these specimens. Resistivity measurements demonstrates early degradation in epoxy only samples compared to graphene loaded ones. The extent of degradation is higher for specimens subjected to electric current compared to oven heated samples. The study is expected to broaden the understanding of using small amounts of graphene (1.4-2.8 wt.% of epoxy) as a filler to abate electric current induced damages in carbon fiber epoxy composites.

TABLE OF CONTENTS

LIST OF TABLES

LIST OF FIGURES

NOMENCLATURE

Abbrevation	Description
CFRP	Carbon fiber reinforced polymer
CF	Carbon fiber
CNT	Carbon nanotube
GNP	Graphene nanoplatelets
CTE	Coefficient of thermal expansion
SPE	Solid polymer electrolyte
PEG	Polyethylene glycol
DMF	N, N- dimethylformamide
UD	Undegraded
OH	Oven heated
ED	Electrically degraded
GO	Graphene oxide
IC	Ionic conductivity
BS	Bath sonication
PS	Probe sonication
TM	Three roll milling
SM	Shear mixing
IFSS	Interfacial shear strength
SFFT	Single fiber fragmentation test
VARTM	Vacuum assisted resin transfer molding

Notation	Description
T_g	Glass transition temperature ($^\circ C$)
σ_c	Compressive strength (MPa)
σ_f	Flexural strength (MPa)
R_r	Transverse resistivity (Ωmm)
R_t	Through thickness resistivity (Ωm)
E_B	Flexural modulus (GPa)
E_A	Activation energy (KJ/mol)
l_c	Critical fiber length (μm)
τ	Interfacial shear strength (MPa)

CHAPTER I

EFFECT OF GRAPHENE ON THE ELECTRICAL DEGRADATION OF CARBON FIBER EPOXY COMPOSITES

1.1 Introduction

1.1.1 Electrical degradation of carbon fiber epoxy laminates

The replacement of metallic components with composites in materials has made them vulnerable to the adverse effects of electric current. This detrimental effect is also pronounced in multifunctional composites like structural supercapacitors, since they are subjected to the repeated applications of electric current. This is primarily attributed to the relatively low thermal and electrical conductivities of composite structures, which necessitates the presence of a conductive skin which could facilitate the rapid exit of electric current [1, 2, 3]. Apart from the direct effects, which include the gradual vaporization of the matrix, breakage of fibers and the subsequent burn off of the laminate, the induced transient voltage developed by the passage of electric current can also damage the electronic systems. Composite manufacturers have devised several attempts to address this issue. This includes connecting metallic meshes to the exterior of the material, bonding resin with metalized fibers, and coating conductive adhesives or films on the surface. Although these methods yield positive effects, they may offset the weight savings offered by these structures. Furthermore, they are hard to repair and may corrode over time [4, 5].

The passage of electric current through the structure coupled with the radiation heating caused by the dielectric breakdown of the surrounding air can lead to the development of a significant amount of heat in the material. Hence improving the thermal conductivities of composites is imperative to abate thermal damage. One way to address this problem

is to use carbon-based fillers with a high surface area which could facilitate the spread of the heat, consequently reducing the damage. Moreover, adding these fillers to the matrix can enhance the multifunctionality of the composite material by improving both the load carrying capacity and the resistance to electric current induced damages [6, 5].

1.1.2 Effect of electrical degradation on different properties

The conductive nature of carbon fibers permits the use of resistance and current in evaluating the damages of CFRP laminates. For example, an inverse relationship exists between electrical resistance and stiffness, and there is a swift increase in resistance when the specimen approaches failure [7]. Irving et al. [8] observed an increase in resistance of CFRP with static and fatigue loading under tensile mode. This change in resistance was attributed to the strain variations in carbon fiber. Studies have also identified that an increase in the magnitude of current can enhance peak load and absorbed energy [9].

The mechanisms of current induced degradation of CFRP are explained based on matrix cracking and the subsequent breakage of carbon fibers [7]. This is caused by Joule heating, Lorentz forces, and delamination, which can lead to debonding and electron hopping between carbon fibers [10]. These results were also supported in the studies of Mall et al. [5], who identified the sequence of current induced failure mechanisms in carbon fiber composites as matrix cracking, followed by delamination, buckling, and fiber breakage.

Furthermore, studies have also reported the development of residual stresses at the interface which can enhance degradation. This is caused by the mismatch in the coefficient of thermal expansion (CTE) between the fiber and the matrix. Although a high CTE permits the matrix to expand, this is often hindered by the fibers with comparatively low CTE, leading to the development of thermal stresses in the matrix [11]. The crosslinking in epoxy can considerably improve its modulus and fracture strength, however its brittle nature can facilitate the development of cracks in these high residual stress fields, eventually leading to failure [12].

The breakdown of epoxy when subjected to an electric field can be explained by the thermal and electromechanical aspects. The former occurs when the heat produced in the epoxy is higher than the heat evacuated (happens at high temperature), consequently leading to structural changes and impairment. The latter involves a reduction in dielectric strength caused by mechanical deformation when epoxy is exposed to an electric field. Identifying critical current density is significant as a sharp increase in temperature is reported above this point which can lead to a deterioration in dielectric properties [13].

The effect of temperature on CFRP specimens is reflected in the changes in mechanical properties and thermal stress [14]. Studies have identified a substantial decrease in mechanical properties of composites with an increase in temperature. In their study on unidirectional carbon composites, Odegard et al. [15] reported a significant drop in elastic constants, shear and transverse strength properties with an increase in temperature. Shenghu et al. [16] identified a substantial reduction in tensile strength at higher temperatures and observed a close correlation between tensile strength and storage modulus. It was also noted that the drop in interlaminar shear strength at elevated temperatures can lead to delamination of the specimen [17].

Degradation of CFRP specimens is anisotropic and depends on the geometry of the specimen [18]. Hence, various methods like, compression test, DMA and conductivity studies can be used to characterize degradation [19]. DMA is a powerful tool to evaluate the viscoelastic properties of a polymer composite. A higher T_g and tan δ of the composite specimen corresponds to a better cross linking and higher heat dissipation capacity, respectively [20]. Compression test is an effective characterization tool to assess the extent of electrical degradation of carbon fiber epoxy laminates with fillers. For example, study [5] reported a 30 to 75 percent drop in compression strength with different fillers. Moreover, a close correlation between compression strength and structural damage was reported in the study. From the literature, it is clear that during electrical degradation, the cumulative effects of electric current and temperature can lead to the damage of the laminate.

1.1.3 Effect of different fillers on properties of carbon fiber epoxy laminates

Some primary requirements to minimize electric current degradation like high electrical conductivity, shielding potential, and high specific surface area can be achieved by adding carbon-based fillers like CNTs and graphene [21]. The surface area of fillers like GNP or CNTs is significantly higher than metallic oxides. This can translate into a larger interphase area between the filler and resin.

Interface strength and the state of dispersion of the filler in the matrix are the critical factors that can determine properties of composites. The physical nature of fillers, for example, the existence of their morphology as bundles and agglomerates instead of individual particles, could lead to a reduction in electrical and mechanical properties. This phenomenon, often termed agglomeration, is addressed through ultrasonication, three roll mill, or shear mixing. Apart from the physical nature, improved interfacial interactions between the filler and the matrix, alignment and high aspect ratio can enhance mechanical and thermal properties. It is also reported that an electrically conductive CFRP with well dispersed additives can lower the electric field [13].

Studies [22] have reported that although CNTs generally have a low percolation threshold compared to graphene, the latter shows better improvement in electrical conductivity. A lower electrical percolation limit (for example 0.5 percent) can be achieved by fillers with a high magnitude of aspect ratio and electrical conductivity [23]. This is ascribed to their ability to form conductive networks, thereby facilitating the transformation of the polymeric behavior from insulating to conducting. However, there has been not much consensus on the electrical percolation limit for fillers and huge variations are reported, for example 0.002 to 7 weight percent for CNTs [24].

The low thermal conductivity of epoxy can be enhanced by adding nanofillers. The thermal conductivity of filler composites depends on the filler loading percent, alignment, dispersion, and most importantly, the thermal resistance between the filler-matrix interface [25]. This is best explained by the concept of phonon, which in simple terms corresponds

to a quantized packet of heat energy responsible for the transmission of heat within the polymer. The addition of fillers minimizes scattering of phonons, leading to their improved transportation and, thus better thermal conductivity [26].

Although a high crosslinking offers distinct advantages like rigidity and good structural strength to epoxy, it could result in low fracture resistance. Fillers like PEG can improve toughness; however, they can significantly reduce the interfacial shear stress and flexural properties of the laminate. Hence selection of fillers and their optimization is critical in the fabrication of polymeric carbon fiber composites.

1.1.4 Graphene as a filler material

Graphene, an allotrope of carbon with a densely packed honeycomb crystal lattice has received considerable interest due to its remarkable mechanical, electrical, and thermal properties. The ability of graphene to strengthen the epoxy matrix is greatly dependent on its state of dispersion and interfacial interaction with the matrix [23]. Hence dispersing graphene in the matrix is a critical aspect of processing. Sonication, magnetic stirring, three roll milling, and their combinations are normally used to achieve dispersion of graphene in epoxy. Kazi et al. [27] identified three roll mill as the most efficient technique to disperse graphene in epoxy. In this process, a high shear stress breaks the agglomerates leading to an improved dispersion. Another route to achieve better dispersion of graphene is through surface modification which includes methods like non-covalent and covalent methods. The former uses stabilizers like surfactants, and the latter involves developing covalent bonds between functional groups.

The improvement in interfacial properties with the addition of graphene to epoxy is reflected in the enhancement of mechanical properties like tensile strength, fracture toughness, Young's modulus, and flexural strength. For example, by using 6 percent GNP in epoxy composites, King et al. [28] reported a 19 percent increase in the tensile modulus (from 2.72 to 3.36 GPa) and a 54 percent decrease in ultimate tensile strength (from 77.6 to 35.5 MPa). This was also supported by the studies of Fukushima et al. [29] with a GNP loading of 3

percent.

Rafie et al. [30] reported over a 30 percent increase in Young's modulus, tensile strength, and fracture toughness of GNP nanocomposites compared to pure epoxy. The improvement was attributed to the enhanced adhesion at the filler-matrix interface caused by an increased surface area of GNP. This was further supported by the study [31], which identified a rise in both flexural modulus and fracture toughness with 1-2 percent GNP loading. An improvement in flexural strength by 18 percent was observed when 0.1 weight percent of covalently functionalized graphene was introduced in epoxy resin [29]. Significant improvement in flexural strength was also reported for carbon fibers coated with GNP owing to an enhanced interfacial region [32] .

In their study, Cho et al. [33] confirmed that addition of GNP by 3 and 5 weight percent could increase the compressive strength of carbon fiber epoxy composites by approximately 10-15 percent. It was also noted that graphene demonstrated better efficacy in repressing interlaminar crack propagation. Interestingly, three orders of magnitude improvement in fatigue life of the composite was reported by adding just 0.2 percent graphene on epoxy [34]. An interesting study [31] combining CNT and GNP in the ratio of 9:1 (0.5 weight percent) in epoxy composite reported better flexural properties than when these fillers were added separately. This synergistic effect was ascribed to the ability of CNT to reduce agglomerations in GNP by virtue of its high aspect ratio and the efficiency of GNP to link effectively with the matrix due to its high surface area.

The effect of T_g with graphene addition is not very clear. This is because they can hinder the polymer chain mobility and enhances the interfacial interactions, consequently leading to an increase in T_g. On the other hand, the ability of graphene to lower the crosslinking density, can cause the T_g to decrease [35]. Similarly, the role of graphene in improving mechanical properties of composites is also not clear. Although most of the studies observed an increase in mechanical properties, a few have also reported no change or deterioration in properties upon adding GNP. The effect of graphene on mechanical properties of composites

is governed by its weight percent (a high graphene percent can lead to poor mechanical properties), dispersion state, interfacial interaction with epoxy, and morphology [36].

The addition of 0.5 and 1.0 weight percent of graphene to epoxy decreased electrical resistance by two folds and had no effect on tensile strength [37]. It has been also reported that graphene can reduce the dimensional changes in composites. This is attributed to its negative CTE (-3.6 to 4.8 $\times$ 10^{-6}/K) and high specific surface area [38, 39]. There is a significant difference in the thermal conductivities of epoxy (0.2 to 0.3 W/mK) and graphene (2000 to 4000 W/mK) and hence the presence of graphene can enhance the development of thermal pathways [40]. The high thermal conductivity of graphene is primarily attributed to its 2 D geometry which facilitates low interfacial thermal resistance. This could, in turn, facilitate the faster removal of heat, one of the principal requirements to reduce thermal damage during electrical degradation.

Studies have reported that adding GNPs could considerably improve the electrical conductivity of composites primarily due to their conductive nature and high aspect ratio. For example, Han et al. [41] reported a considerable increase in conductivity at 0.63 weight percent of GNP. Significant improvements in thermal, electrical conductivity and flexural strength were reported when 20 percent exfoliated graphite was added to epoxy resin [42]. By using similar weight percent of chemically modified graphite flakes another study [40] reported an increase in thermal conductivity of epoxy from 0.2 to 4 W/mK. However, it has to be noted that compared to the exponential increase in electrical conductivity, the improvement in thermal conductivity values on graphene addition is modest.

Literature suggests that there is no consensus in the thermal and electrical conductivity percolation threshold. Broadly, it can be noted that thermal percolation thresholds have been significantly high compared to electrical threshold. For example, studies reported a thermal percolation threshold of 30 and 17 weight percent graphene loading [43, 44]. On the other hand, studies have used 0.3 to 0.9, 1,2, 5, and 8 percent graphene weight and reported increased electrical conductivity [27].

Based on the literature review, it is clear that most of the research on the electrical degradation of polymeric composites covered both the qualitative and quantitative aspects of changes in mechanical properties and degradation mechanisms. Furthermore, several investigations were performed to analyze the efficiency of graphene as a filler material in polymer composites, both in terms of property enhancement and improved dispersion. However, limited studies discuss the role played by graphene on epoxy matrix and how it affects the electrical, mechanical, and viscoelastic properties of epoxy based carbon fiber reinforced polymers, particularly under the application of electric field. The correlation between these properties and a real time monitoring of resistance and temperature is important to set a benchmark in improving materials for applications involving electric current.

1.1.5 Objective of the study

The goal of this research is to improve the multifunctional properties of carbon fiber epoxy laminates to efficiently counter the degradation caused by electric current. This will be accomplished by identifying significant changes in the electrical, mechanical, and thermal properties of carbon fiber epoxy laminates when loaded with different graphene concentrations (0.7, 1.4 and 2.8 weight percent of matrix). For achieving the objective, cross-ply laminates are subjected to low density electric field by passing direct current. Electrical and thermal properties are continuously monitored using an in-house experimental setup, and mechanical properties; compressive and flexural strengths are determined in accordance with ASTM standards. To analyze the thermal and dielectric effects of electric current, undegraded, oven heated, and electrically degraded samples are considered for each measurement. The extent of degradation is characterized using viscoelastic and resistivity measurements. The study is expected to broaden the understanding of using graphene as a filler to subside electric current induced damages in carbon fiber composites particularly for energy storage applications.

1.2 Materials, experimental set up and methodology

1.2.1 Materials

All chemicals were used as received unless otherwise stated. EPON 862 epoxy resin and EPIKURE 3274 curing agent were manufactured by Hexion ™ (Hexion, Columbus, Ohio) and supplied by Miller-Stephenson ™ (Miller Stephenson, Danbury, Connecticut). Carbon fibers (UNI-4 3IM7 HexTow ™ pan based 12K continuous carbon fiber) were manufactured by Hexcel ® (Hexcel, Stamford, Connecticut). GNP was supplied by XG Sciences-Grade M with an average particle diameter of 25 µm (XG Sciences, Lansing, Michigan). Three roll mill was purchased from Torrey Hills Technologies ® (Make-Torrey Hills Technologies LLC, Model TM-65, San Diego, California). Three roll mill was performed 20 times.

1.2.2 Experimental setup

Hand layup technique was used to make the composite (figure 1). The laminate was a standard cross-ply comprising 12 plies. Carbon fibers of dimension 300 mm × 300 mm were cut in all the cases. The resin was epoxy, epoxy with 0.7, 1.4 and 2.8 weight percent graphene for different laminates. The epoxy-graphene mixture was kept for mechanical stirring for 24 hours, followed by three roll mill for 20 times. The epoxy and the hardener were prepared in the ratio of 5:2.

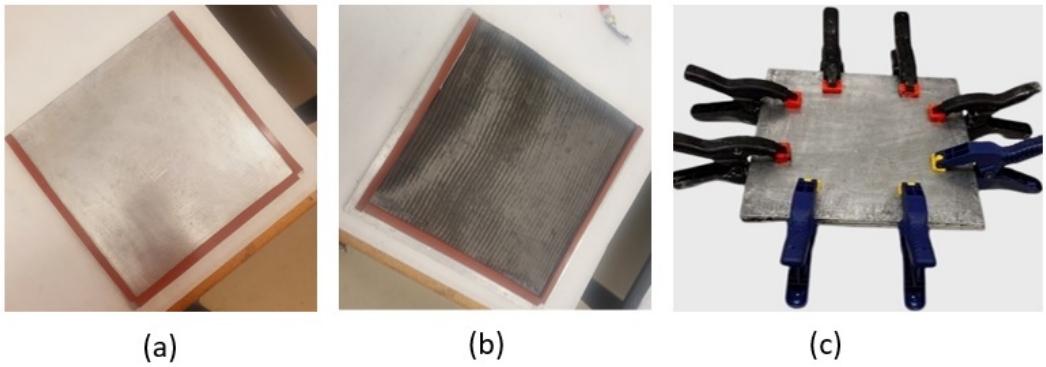

Figure 1: Hand layup set up (a) aluminum base plate with spacers (b) carbon fiber plies stacked on the base plate (c) clamps for holding the base plate tight after layup.

Mold release was applied on an aluminum plate, and carbon fiber was placed on its surface. The resin was painted onto the surface of carbon fiber using a brush. A steel roller was used to ensure uniform resin on the surface of carbon fiber. Another ply was placed above this, and the process continued till all the twelve plies were stacked between the aluminum plates. Clamps and spacers were used to ensure rigidity and to prevent overflow of the resin. The setup is left at ambient temperature for 48 hours. The laminate was then removed from the mold.

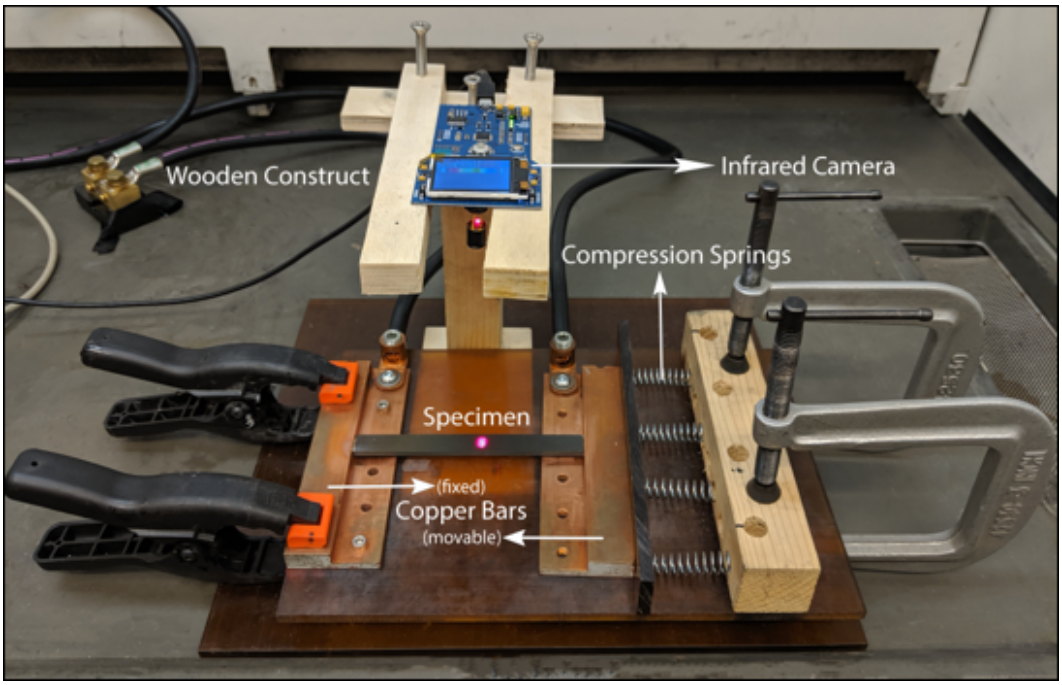

Figure 2: Electrical degradation experimental setup.

The schematic of the experimental setup used in the study is shown in figure 2. It consists of a DC power source (6031 A, HP-Agilent, California), a real-time temperature monitoring system (MLX90621, Melexis Inc, New Hampshire), and an electrode fixture. A detailed explanation of the technique can be found in the study [3]. The variations in voltage and current were logged using a visual basic program, while that of temperature was recorded using an arduino board. Although the temperature was recorded along the sample in twelve segments, only the average midspan temperature (segments 4 to 9) was used in the analysis. This is because the segments at extreme ends may be subject to contact resistance heating.

1.2.3 Methodology

Specimens of dimensions 140 × 13 mm were cut from the laminate using a tile saw (MK-370, MK Diamond Products, Torrance, California). The edges of the coupons were smoothened with sandpaper of grit size 400. Electrically conductive epoxy (Duralco 120, Cotronics, New York) was applied on the edges, and the specimens were left at ambient temperature for 24 hours. Efforts were made to check the orthogonality of the edges and to ensure the smoothness of the silver paste on the edges. The T_g of the undegraded carbon fiber epoxy sample was determined as 53.8 °C using dynamic mechanical analysis (DMA-Q 8000, TA Instruments, Delaware). By performing several trial runs, a critical current density of 46 kA/m^2 was identified, at which no burn off the laminate was recorded.

The samples in all the cases (epoxy, graphene-0.7, graphene-1.4, and graphene-2.8) were subjected to a constant current density of 46 kA/m^2 for 3 hours. The voltage and temperature behavior were monitored during the degradation process. To differentiate the effect of thermal and electrothermal behavior, a few samples in each case were also exposed to isothermal conditions in an air oven (1350 FM, VWR International, Pennsylvania). The average temperatures of the samples after electrical degradation were replicated in the oven. Hence the epoxy, graphene-0.7, graphene-1.4 and graphene-2.8 specimens were oven heated to 88, 72, 78 and 57 °C respectively.

The viscoelastic properties; T_g and tan δ of the samples were characterized using DMA. A frequency of 1 Hz and dual cantilever beam mode was used for the analysis. The peak of the tan δ-temperature curve was used to determine the T_g. Combined loading compression (CLC) and three-point bend test were conducted to determine the compression and flexural strengths. They were performed in accordance with ASTM-D6641 and ASTM-D790 standards, respectively. These tests were carried on a electromechanical testing system (Make-5567, Instron Corporation, Norwood, Massachusetts). DC resistivity was measured along the through-thickness direction by applying a constant voltage of 10 V and recording the variation in current using a multimeter (Make-Mastech MS8268, Pennsylvania).

1.3 Results and Discussion

1.3.1 Resistance profile

The variation of resistance against time for epoxy, graphene-0.7, graphene-1.4 and graphene-2.8 weight percent exposed to a current of 46 kA/m^2 for 3 hours is demonstrated in figure 3. From the figure, it is clear that the non-conducting character of epoxy can be improved by adding graphene.

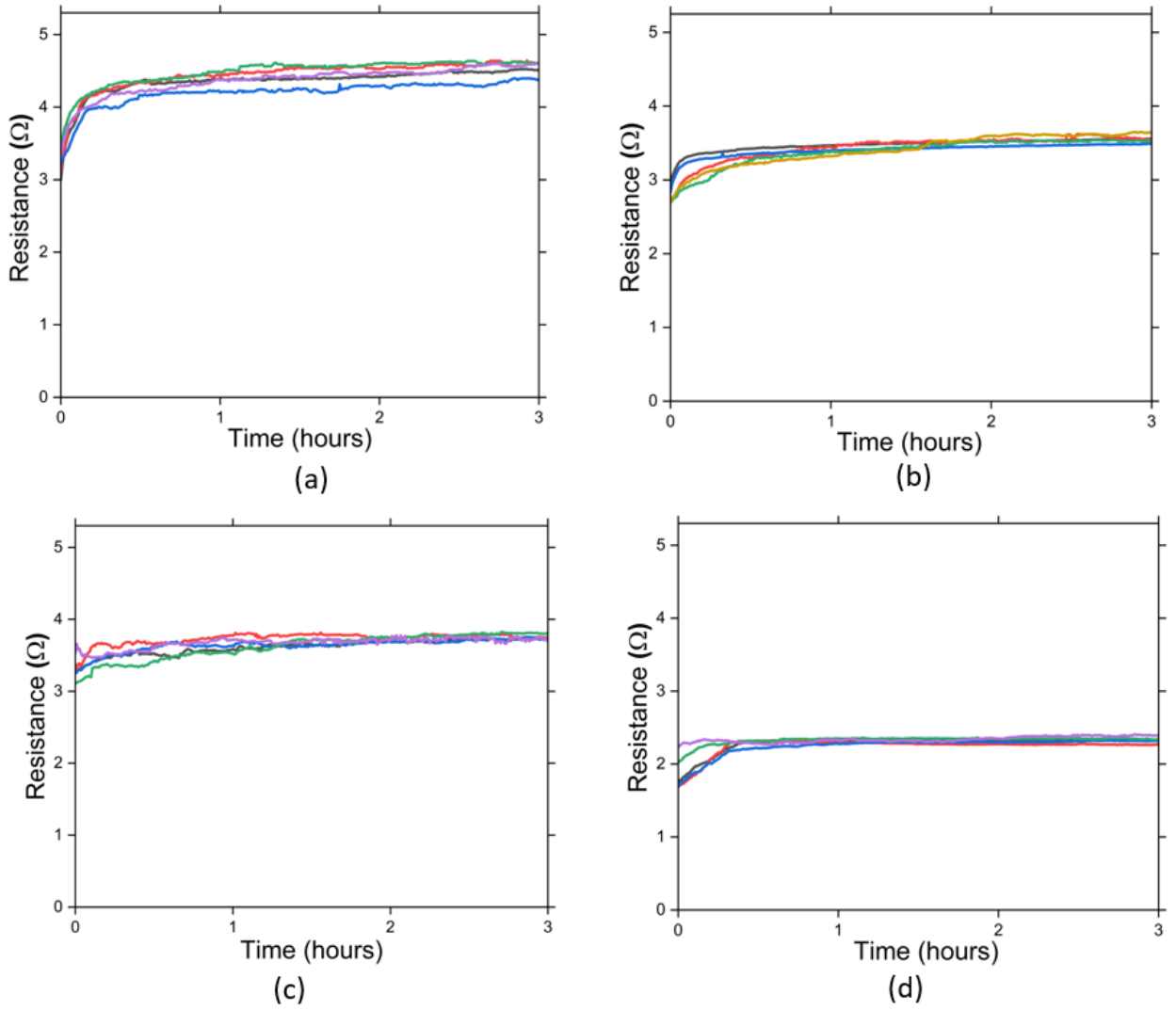

Figure 3: Variation of resistance against time (a) epoxy (b) graphene-0.7 (c) graphene-1.4 (d) graphene-2.8

The resistance profile of the epoxy sample can be divided into two regimes - an initial

rise followed by a stable region. The initial rise in resistance can be explained by the positive temperature coefficient of carbon fibers. When electric current is passed through the sample, Joule heating occurs, leading to the decomposition of epoxy. This initial increase in resistance is followed by a more stable regime due to the dielectric breakdown caused by the applied potential [3]. This is regarded as an irreversible phenomenon and can lead to the development of conduction pathways. The resistance is further lowered as the decomposition of epoxy can lead to more significant contact between carbon fibers. It was also noted that the time taken for all the samples to arrive at a stable regime was not identical. This inconsistency is attributed to their micromechanical damage, anisotropy, and the time needed to overcome Joule heating.

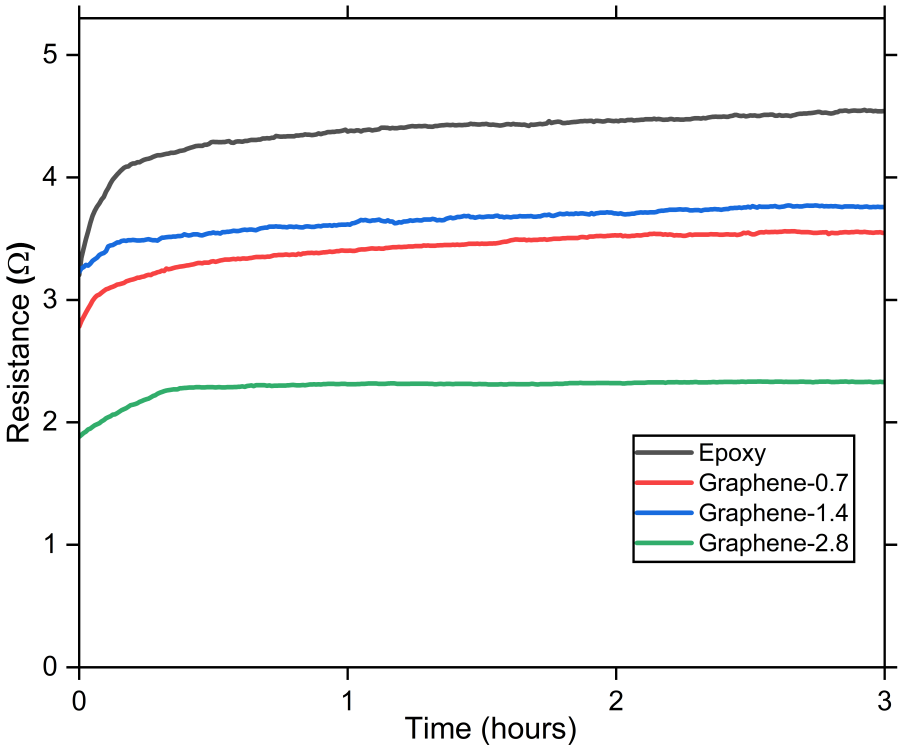

Figure 4: Average variation of resistance against time

The combined average resistance-time characteristics of all the cases is illustrated in figure 4. From the figure, it is clear that the resistance of the specimen was lowered by adding GNP. In other words, the CFRP specimen became more conductive with the addition of

GNP. As evident from the figure, samples with a GNP content of 2.8 percent demonstrated the maximum decrease in resistance.

Table 1 indicate the average resistance of different specimens at the beginning, first, second and third hours of the degradation process. After three hours, almost a fifty percent drop in resistance occurred for the graphene-2.8 specimens. Furthermore, compared to epoxy there is a significant reduction in resistance for both graphene-0.7 and graphene-1.4 samples.

Specimen	Resistance (Ω)				
	0 hr	1 hr	2 hr	3 hr	Reduction (%)
Epoxy	3.20	4.38	4.46	4.54	-
Graphene-0.7	2.78	3.40	3.53	3.55	22
Graphene-1.4	3.23	3.61	3.71	3.76	17
Graphene-2.8	1.88	2.31	2.32	2.33	49

Table 1: Average resistance at different time intervals.

The electrical conduction of a filler based composite depends on the amount of filler and can be explained on the basis of percolation theory. According to this, there exists a critical filler content termed as percolation threshold, below which electron paths are absent and above which multiple electron paths exist. In other words, below the percolation threshold, electrical conduction is realized primarily by the matrix (due to the contact resistance between the particles) [45]. Adding conductive fillers to their percolation limit can significantly reduce resistance, primarily attributed to their ability to form conducting clusters. This change becomes irreversible under the application of electric field due to dielectric breakdown and the consequent formation of conductive pathways [46]. Moreover, the contact resistance between GNP also decreases with an increase in filler content. This is ascribed to the decrease in thickness of epoxy between GNP, consequently leading to the formation of more conducting clusters [27]. However, identification of an electrical percolation threshold can be often challenging as it is formed only under an optimum distribution and a right dispersion.

Apart from the percolation theory, the increase in conductivity upon the addition of graphene can also be described by the lattice structure of graphene and its chemical reactivity. Graphene is sp^2 hybridized with half filled π orbitals situated above and below its planes. The presence of delocalized electrons in these orbitals and their subsequent overlapping favors conductivity. Moreover, the presence of incomplete bonds on the edges enhances its reactivity; for example the interaction of π electron cloud of graphene with benzene ring of epoxy. Along with this, exceptionally high surface area of graphene facilitates the development of a strong matrix-filler interface. Thus, the inherent conductive nature of graphene coupled with its high reactivity and peculiar structure, helps to establish a strong interaction with epoxy, consequently reducing the resistance of the laminate.

It was expected that graphene-1.4 should exhibit a lower resistance compared to graphene-0.7 specimens. However, this was not the case, and the resistance in graphene-1.4 was slightly more than graphene-0.7 samples. This peculiar behavior can be explained by dispersion and consequent agglomeration of GNP in epoxy resin for graphene-0.7 specimens. Studies have identified that agglomeration can lead to an unexpected increase in conductivity since it can facilitate the transport of electrons through the tunneling phenomenon. However, it has to be noted that such an effect is pronounced only at lower concentrations and for fillers with high aspect ratios like graphene [47, 48, 49] .

A fully effective dispersion occurs when all GNPS are separately layered. The Vander Waals forces in graphene can cause it to agglomerate, thereby affecting its solubility in solvents leading to poor dispersion [50]. Studies [51] have also identified selective localization of graphene rich-scarce regions within the composite due to phase separation and agglomeration. Thus, a higher degree of agglomeration and selective localization of graphene within the specimens could have probably led to the decreased resistance of 0.7 weight percent sample compared to 1.4 weight percent. Since no sharp drop in resistance was observed at 1.4 percent graphene loading, it can be concluded that the electrical percolation threshold was not attained at 1.4 percent. The conductivity before attaining percolation threshold limit

is primarily attributed to electron tunneling, connecting the GNP through the filler-matrix interface.

1.3.2 Temperature profile

The variation of temperature against time for epoxy, graphene-0.7, graphene-1.4 and graphene-2.8 weight percent exposed to a current of 46 kA/m^2 for 3 hours is demonstrated in figure 5.

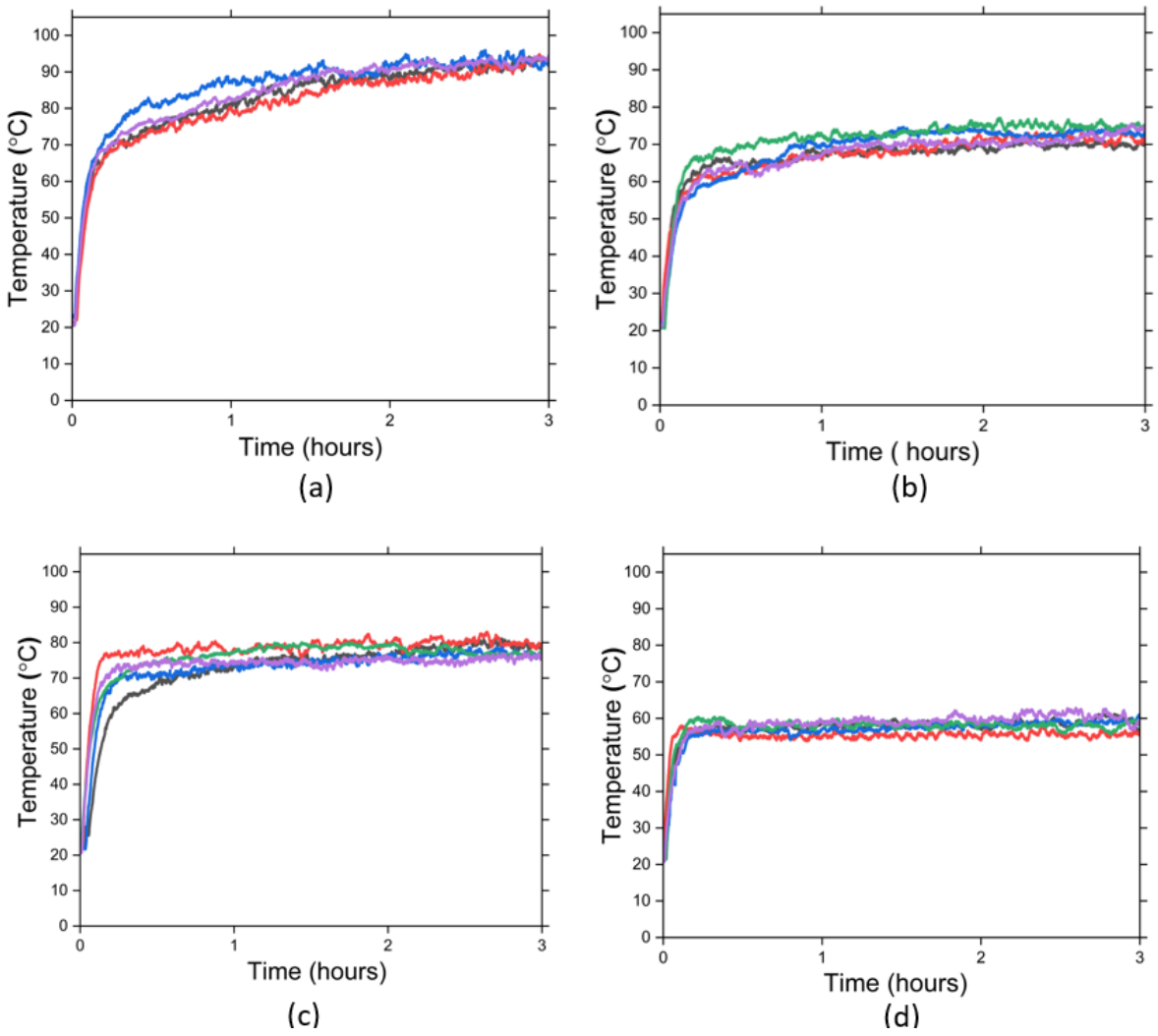

Figure 5: Variation of temperature against time (a) epoxy (b) graphene-0.7 (c) graphene-1.4 (d) graphene-2.8

The trend in the variation of temperature is similar to the variation of resistance. The

differences in the temperature profile of the samples in a given set are attributed to differences in resistances, thermal mismatch, and the presence of different numbers of conducting pathways in each of them.

The initial rapid temperature rise is caused by the positive temperature coefficient of carbon fibers. This is followed by Joule heating. The linear variation of heat and resistance in the sample applies in this stage. It is also expected that the increase in temperature could enhance the motion of epoxy, restricting conduction. The rapid rise is followed by a stable temperature regime attributed to the dielectric and thermal breakdown of epoxy. The effects of Joule heating and the consequent increase in temperature reduces over time due to the development of conducting channels assisting current flow.

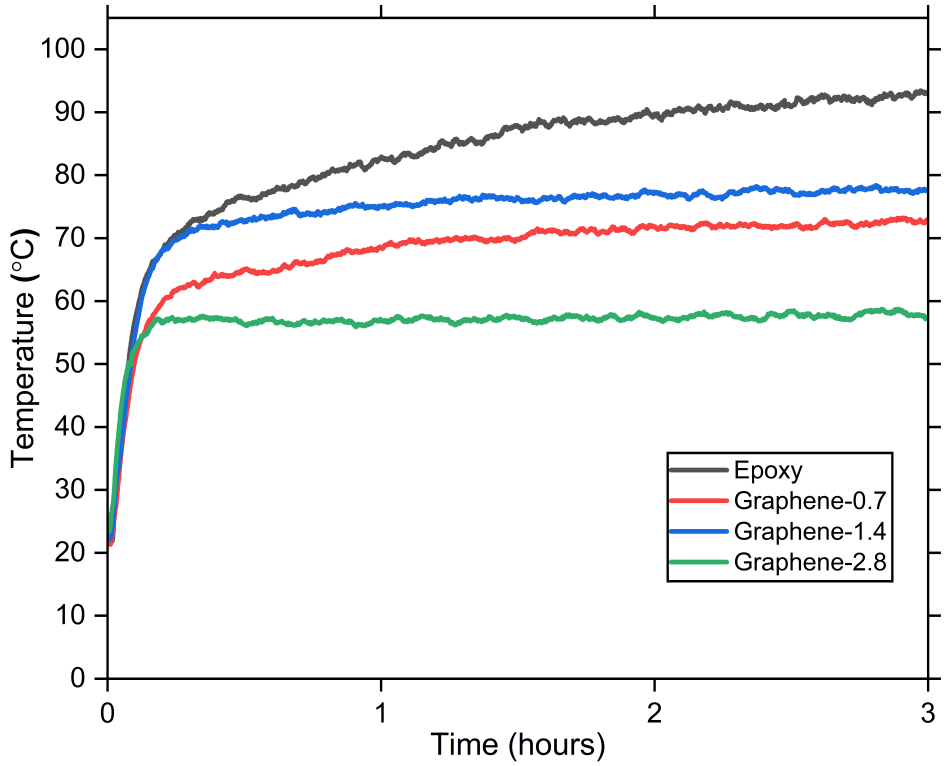

Figure 6: Average variation of temperature against time

The combined average temperature-time characteristics of all the cases is illustrated in figure 6. From the figure, it is clear that the temperature of the specimen was lowered by adding GNP. As evident from the figure, samples with a GNP content of 2.8 percent

demonstrated the maximum decrease in temperature.

Table 2 indicate the average temperature of different specimens at the beginning, first, second and third hours of the degradation process. After three hours, almost a forty percent drop in temperature occurred for the graphene-2.8 specimens. Furthermore, compared to epoxy there is a significant reduction in temperature for both graphene-0.7 and graphene-1.4 samples.

Specimen	Temperature (°C)			
	1 hr	2 hr	3 hr	Reduction (%)
Epoxy	82.9	89.6	93.1	-
Graphene-0.7	68.5	71.8	72.6	22
Graphene-1.4	75.1	77.4	77.5	17
Graphene-2.8	57.0	57.3	57.1	39

Table 2: Average temperature at different time intervals.

The reduced temperature of graphene loaded specimens is attributed to the exceptionally high thermal conductivity of graphene. The thermal conduction in polymers is explained by the transportation of phonons. The presence of interfacial thermal resistance can lead to phonon scattering at the interface. Although carbon fibers have a high thermal conductivity along the fiber direction, the presence of epoxy could lead to a significant reduction in transverse conductivity. Consequently, this impedance mismatch can pave way for phonon scattering. Meanwhile, the two-dimensional structure of graphene, coupled with its large surface area and wrinkled structure, can also lead to a lower interfacial thermal resistance by improving transverse conductivity. Furthermore, the addition of graphene could reduce the inter filler space in the matrix and facilitates the formation of thermal pathways under electric fields. An increase in temperature can also pave way for the development of small sized cracks which may lead to diffusion pathways [52].

Along with its exceptionally high thermal conductivity value, the negative coefficient of thermal expansion (CTE) of graphene could minimize the dimensional changes of the polymers by reducing the overall CTE of the composites. This is different from carbon fiber

epoxy composites, where there is a considerable difference between the CTE of epoxy and carbon fiber. Such a difference could lead to the development of residual thermal stresses paving way for crack propagation and subsequent degradation. On the other hand, the addition of graphene could minimize the residual thermal stresses considerably.

1.3.3 Dynamic mechanical analysis

The dynamic mechanical analysis (DMA) results supports the previous observation that addition of graphene could lower both the resistance and temperature of the specimen. The two parameters, T_g and tan δ were studied. Table 3 demonstrates the variation in T_g for undegraded (UD), oven heated (OH) and electrically degraded (ED) specimens. From the table it is clear that there is a significant improvement in the T_g for graphene loaded samples. This increase in T_g is attributed to the restriction of molecular motion and a subsequent decrease in free volume upon the addition of GNP. This can lead to a stronger bonding and hence improved load transfer at the interface. Furthermore, it is important to note that a higher T_g facilitates better crosslinking, leading to a tighter network and an improvement in compressive properties.

Specimen	T_g-UD °C	Increment %	T_g-OH °C	Increment %	T_g-ED °C	Increment %
Epoxy	53.8 ± 0.9	-	51.4 ± 0.5	-	50.7 ± 0.9	-
Graphene-0.7	58.9 ± 0.3	9	56.9 ± 0.4	11	54.9 ± 0.1	8
Graphene-1.4	61.6 ± 0.7	14	58.9 ± 1.0	15	56.7 ± 0.7	12
Graphene-2.8	67.1 ± 0.7	25	66.8 ± 0.7	30	61.7 ± 0.8	22

Table 3: Variation of T_g for different specimens.

When CFRP is held at temperatures above its T_g, it can affect the dielectric due to changes in its viscoelastic properties and matrix softening. This is because, at temperatures above T_g, the formation of free radicals or processes like recombination of polymer chains or chain scission occurs. Applying an electric field under this state can cause the development of conduction current and ionization of the polymer. This can accelerate Joule heating and

avalanche breakdown, leading to the premature breakdown of the dielectric [53, 54].

The variation of tan δ against temperature for all the samples is illustrated in figure 7. From the figure, it is clear that electrically degraded samples have a higher tan δ followed by oven heated and undegraded specimens. The peak of tan δ was used to determine T_g.

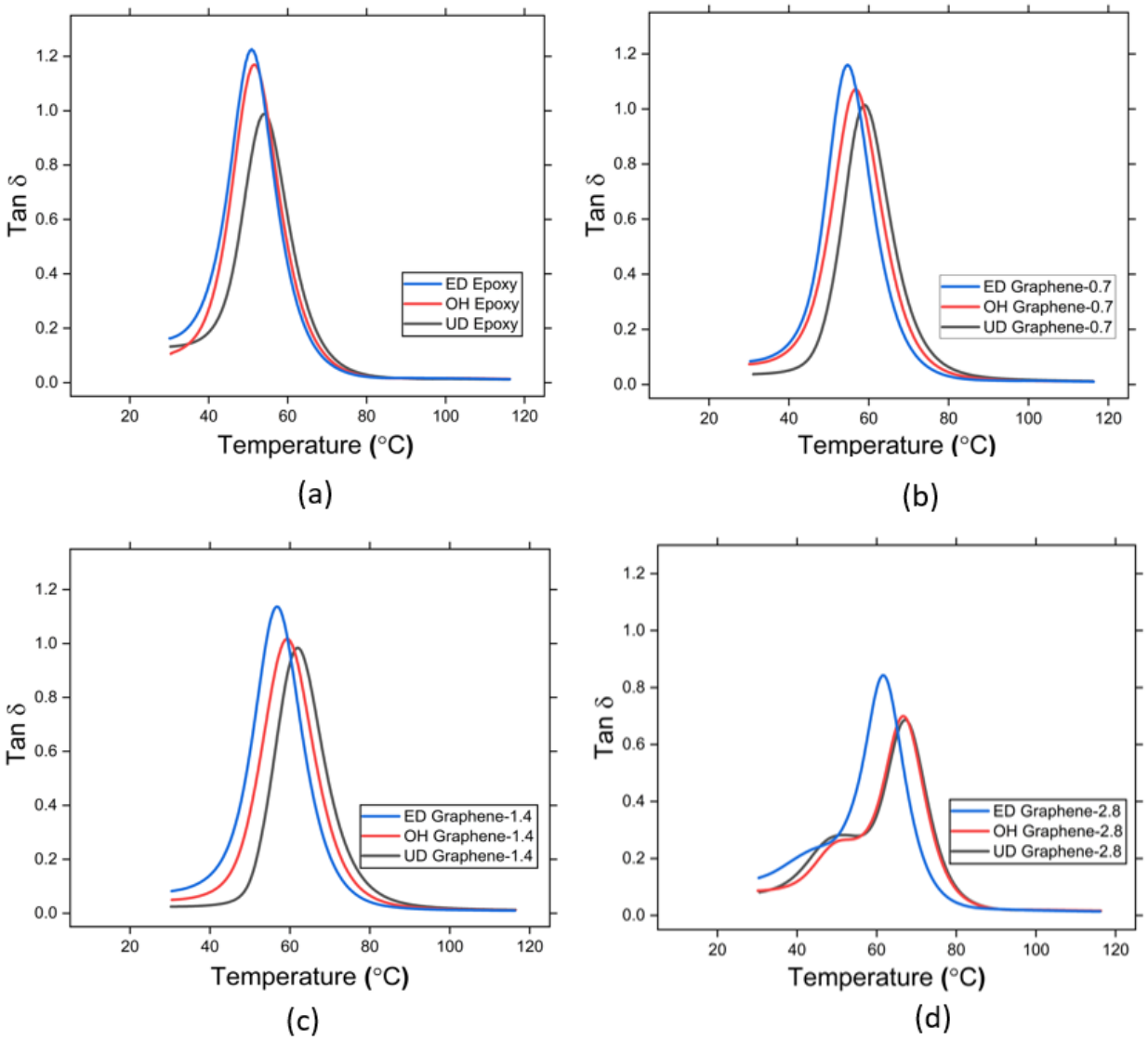

Figure 7: Variation of tan δ against temperature (a) epoxy (b) graphene-0.7 (c) graphene-1.4 (d) graphene-2.8

On comparing the samples, it was noted that T_g was highest for undegraded specimens, followed by oven heated and electrically degraded ones. Furthermore, with the addition of graphene, there is a shift of peaks towards higher temperature, revealing an increase in T_g.

It is interesting to note that there is an intermediate bump in the tan δ-temperature graph of graphene-2.8 specimens. This is possibly due to the formation of a polymer blend leading to relaxations at different temperatures.

Table 4 demonstrates the variation in tan δ for undegraded, oven heated and electrically degraded specimens. A higher tan δ corresponds to a greater energy dissipation potential and a lower load bearing capacity. It is also a measure of viscous to elastic response of a material. An increase in tan δ also implies a reduction in interfacial bonding of the fiber and matrix. This is possibly due to the higher molecular motion at the epoxy-carbon fiber interface.

Specimen	tan δ-UD	Reduction %	tan δ-OH	Reduction %	tan δ-ED	Reduction %
Epoxy	1.00	-	1.18	-	1.24	-
Graphene-0.7	1.01	+1	1.07	9	1.16	7
Graphene-1.4	1.02	+2	1.04	12	1.15	8
Graphene-2.8	0.71	29	0.71	40	0.85	32

Table 4: Variation of tan δ for different specimens.

Compared to undegraded samples, oven heated and electrically degraded samples are subjected to the effects of temperature leading to the development of thermal stresses. Moreover, electrically degraded samples in all the cases are also subjected to Joule heating which can further lead to energy dissipation accounting for their higher tan δ values. From the DMA results, it is clear that GNP loaded samples have a higher T_g and low variations in tan δ, which confirms that addition of GNP to the composite enhances the durability and ability to withstand electric current induced damages.

1.3.4 Mechanical properties

The mechanical properties investigated in the research are the compressive strength (σ_c) and flexural strength (σ_f). The compressive and flexural strengths for undegraded, oven heated, and electrically degraded samples are tabulated in table 5 and table 6.

A comparison of the compressive and flexural strengths of epoxy samples with respect to GNP loaded specimens reveals that there is an increase in these properties with the addition of graphene. This increase is primarily attributed to the high surface area of GNP, leading to an enhanced adhesion at the graphene-epoxy interface. Moreover, the high chemical reactivity of graphene due to the presence of incomplete bonds on its edges can improve the mechanical properties of epoxy, consequently facilitating a stronger matrix-fiber interface and thus a delayed fiber buckling.

Specimen	σ_c-UD MPa	Increment %	σ_c-OH MPa	Increment %	σ_c-ED MPa	Increment %
Epoxy	189 ± 15	-	176 ± 10	-	161 ± 11	-
Graphene-0.7	202 ± 16	7	197 ± 16	12	182 ± 8	13
Graphene-1.4	217 ± 9	14	203 ± 15	15	194 ± 12	21
Graphene-2.8	203 ± 9	7	192 ± 12	9	187 ± 12	16

Table 5: Variation of compressive strength for different specimens.

It is also important to note that the improvement in mechanical properties with the addition of graphene is also dependent on the efficiency of dispersion, as poor dispersion can lead to agglomeration, paving the way for the development of voids in the interface. The decrease in compressive properties of 2.8 weight percent compared to 1.4 weight percent graphene loaded samples can be explained by the attainment of a threshold between 1.4 and 2.8 weight percent. The addition of GNP beyond this limit may lead to agglomeration and defects. This can lead to the development of voids leading to a drop in compressive properties. On the other hand, an increase in flexural strength is primarily attributed to the development of a stronger interface upon the addition of graphene. This is possibly due to improved mechanical interlocking and chemical bonding at the interface.

It was observed that compared to undegraded samples; oven heated, and electrically degraded samples experienced a decrease in compressive and flexural strength. The relatively higher drop for electrically degraded compared to oven heated samples reveals the adverse effect of electric current on mechanical properties. Moreover, the result also suggests that

Specimen	σ_f-UD MPa	Increment %	σ_f-OH MPa	Increment %	σ_f-ED MPa	Increment %
Epoxy	133 ± 13	-	112 ± 14	-	87 ± 9	-
Graphene-0.7	151 ± 13	14	140 ± 8	25	131 ± 11	51
Graphene-1.4	167 ± 10	26	155 ± 10	39	143 ± 13	66
Graphene-2.8	198 ± 14	49	175 ± 18	56	163 ± 7	89

Table 6: Variation of flexural strength for different specimens.

degradation by both thermal and matrix effects can lead to a drop in mechanical properties.

1.3.5 Resistivity measurements

Tables 7 and 8 demonstrates the variation in transverse resistivity (R_r) and through-thickness resistivity (R_t) for undegraded, oven heated, and electrically degraded specimens. It is interesting to note that that compared to epoxy, graphene-0.7 samples showed an increase in resistivity. This unique behavior is possibly due to agglomeration leading to the development of graphene rich- scarce region in the sample [51, 50].

Specimen	R_r-UD (Ωmm)	Change %	R_r-OH (Ωmm)	Change %	R_r-ED (Ωmm)	Change %
Epoxy	28.1 ± 1.4	-	29.8 ± 0.5	-	25.7 ± 1.6	-
Graphene-0.7	28.6 ± 1.2	+2	31.6 ± 0.8	+6	29.9 ± 1.3	+16
Graphene-1.4	24.5 ± 0.7	-13	27.2 ± 0.9	-9	25.2 ± 1.4	-2
Graphene-2.8	21.4 ± 1.0	-24	24.5 ± 1.4	-18	22.7 ± 1.0	-12

Table 7: Variation of transverse resistivity for different specimens.

Specimen	R_t-UD (Ωm)	Change %	R_t-OH (Ωm)	Change %	R_t-ED (Ωm)	Change %
Epoxy	115 ± 21	-	194 ± 48	-	268 ± 37	-
Graphene-0.7	128 ± 22	+11	338 ± 64	+74	377 ± 67	+40
Graphene-1.4	61 ± 17	-47	130 ± 23	-33	211 ± 18	-21
Graphene-2.8	73 ± 12	-37	185 ± 19	-5	263 ± 27	-2

Table 8: Variation of through-thickness resistivity for different specimens.

From table 7, it can be noted that the transverse resistivity of electrically degraded epoxy samples was low compared to oven heated and undegraded specimens. This is possibly due to early dielectric degradation occurring in epoxy compared to graphene loaded samples. After

dielectric breakdown, the conducting nature of the polymer is expected to increase due to the development of conductive pathways [55, 56]. Moreover, the relatively high temperature of epoxy compared to graphene loaded samples could pave the way for the accelerated thermal breakdown of the dielectric favoring the rapid formation of conductive channels [3]. Furthermore, the relatively weaker interface of epoxy may facilitate the expeditious degradation of the interface region, leading to contact between carbon fibers and a consequent reduction in transverse resistivity. Nevertheless, for graphene loaded samples, it can be noted that the transverse resistivity of undegraded samples was lower compared to electrically degraded specimens. This suggests the ability of these specimens to abate the degradation of the dielectric.

From table 8, it is clear that electrically degraded samples, in all cases, experienced an increase in through-thickness resistivity. This is ascribed to a high degree of delamination in the specimens under the application of the electric field. The relatively low values of oven heated compared to electrically degraded specimens confirms Joule heating and subsequent degradation of the dielectric. Meanwhile, the higher values of oven heated compared to undegraded specimens affirms that temperature is also a significant factor affecting through-thickness resistivity and hence delamination.

1.4 Conclusion and future work

The study investigated the effect of adding graphene as a filler material to reduce the degradation of carbon fiber epoxy laminates when subjected to low density direct current. Different weight percent of graphene (0.7, 1.4, and 2.8) were added to epoxy to understand the variation in resistance, temperature, T_g, tan δ, compressive strength, flexural strength, and resistivity. To ensure efficient dispersion, the epoxy-graphene mixture was subjected to mechanical stirring followed by three roll mill. Cross-ply laminates made by hand layup technique were cut into rectangular specimens and was subjected to a current of 46 kA/m^2 for three hours. An in-house experimental setup monitored real-time variations in temperature

and voltage. To differentiate the effect of temperature and electric current, a few samples were also exposed to isothermal conditions in an oven.

Resistance of the specimen dropped by 17 to 49 percent after three hours upon the addition of graphene. The decrease in resistance is attributed to percolation, unique structure, and the reactivity of graphene, facilitating an efficient interaction with epoxy. Similar to resistance, the addition of graphene led to a significant drop in temperature (17 to 39 percent). This is ascribed to the high thermal conductivity of graphene, paving the way for reduced interfacial thermal resistance and residual thermal stresses. Graphene-loaded samples also showed significant improvement in T_g (9 to 25 percent), suggesting an improved crosslinking and efficient load transfer at the interface. The low variations in tan δ were also noted for these samples revealing their higher energy storage capabilities. The addition of graphene increased both the compressive and flexural strength of the laminate primarily due to the development of a strong fiber-matrix interface. The extent of degradation was higher for specimens subjected to electric current compared to oven heated samples revealing the relative effects of both electrical and thermal effects. The reason for the anomalous behaviour at 0.7 percent graphene has to be further investigated with respect to agglomeration and tunneling at low concentration. From the study, it can be concluded that the addition of a small amount of graphene (1.4 to 2.8) can lead to significant improvements in the electrical, crosslinking and mechanical properties of CFRP.

Future research works could investigate the extent of dispersion and identify agglomerations at different graphene loadings. The effect of aligning GNP [57] and using different particle sizes is another area of interest. The sequence and changes in degradation mechanisms can be investigated as a function of different current densities. A numerical model correlating the damage, electric resistance, and temperature can be used to optimize thermal and electrical percolation limits. This can be further extended by incorporating a finite element analysis to predict electrical and thermal variation distributions at different regions of CFRP.

CHAPTER II

A STUDY ON THE EFFECT OF DIFFERENT PROCESSING TECHNIQUES ON IONIC CONDUCTIVITY OF SOLID POLYMER ELECTROLYTES

2.1 Introduction

2.1.1 Solid polymer electrolytes with graphene oxide

A solid polymer electrolyte (SPE) is made of salts like sodium or lithium dispersed in a polar polymer matrix. The use of SPE in the development of energy storage devices is on the rise, as they are safer due to reduced reactivity, flexibility, offer better ionic conductivity (IC) and mechanical strength, and prevent electrolytic leakage compared to conventional organic solvent-based electrolytes. Moreover, the addition of functional fillers like graphene oxide (GO) to the SPE opens a further superior advancement in their properties [58]. Good dispersion of the polymer with the filler material is also imperative in the improvement of electrical and mechanical properties. Several studies have confirmed that the quality of dispersion greatly depends on the equipment, mixing time and mixing velocity [59]. Thus, formulating ideal processing stages of SPE with filler material is crucial in the development of solid polymer electrolytes (SPE) [60].

GO is oxidized from graphene and has been a popular filler material primarily due to its ease of manufacture, good mechanical properties, and high thermal conductivities [61]. For example, adding just 0.1 and 0.5 weight percent of GO to pure epoxy increased fracture toughness by 75 percent and storage modulus by 12 percent, respectively [62, 63]. GO is made

of layered structures with oxygen-containing functional groups like hydroxide and epoxide along the C-C basal edges and planes. They are held together by weak Van der Waals forces [64]. These forces could also facilitate dispersibility and enhance hydrogen bonding and interfacial interactions between GO and the polymer matrix. Exfoliation is defined as the process of overcoming the Van der Waals forces between different layers, thereby achieving monolayers of GO.

2.1.2 Ultrasonication- A tool for better dispersion

Fabrication of GO based electrolytes generally involves ultrasonication treatment during processing stage [65, 66, 67]. This is primarily attributed to the efficacy of this method in exfoliating multilayered GO to singular GO sheets, accompanied by the reduction in their size. Ultrasonication is generally achieved using devices like bath or probe sonicator. The basic working principle of a bath sonicator can be best described by the development of alternating pressure cycles (compression and rarefaction), bubble formation and collapse. During compression cycle, bubbles are developed by the energy transferred from the piezoelectric transducers present under the oscillating tank bottoms. The implosion of the bubbles during the rarefaction cycle agitates the liquid, leading to interparticle collisions and collisions within the walls. This can further cause the development of tensile stress, subsequently leading to cracks in particles and their separation [68, 69]. In a probe sonicator, the cavitation process is caused by the rapid vibration of the tip. The amplitude measures the probe's vibrational expansion and contraction. The probe diameter, amplitude and time are the three important parameters that can affect the processing of the sample [70].

In their study [71] to synthesize gel electrolytes with GO and polyethylene glycol (PEG), different weight percentages of GO (0 to 0.7 percent) were mixed with PEG and subjected to ultrasonication for 2 hours. Qi et al. [72] used one hour ultrasonication to prepare PEG-GO nanocomposites (0.5 to 8 percent GO weight). In another study [73] to determine the IC of a GO-polyethylene oxide (PEO) SPE, Cheng et al. sonicated GO in N, N- dimethylformamide

(DMF) using an ultrasonic bath sonicator for 1.5 hours to ensure uniform dispersion. Using TEM images, the research reported a lateral size of 200-500 nm for GO nanosheets suggesting their improved exfoliation after sonication in DMF.

Javaid et al. [74] performed ultrasonication of SPE composed of diglycidyl-ether of bisphenol-A epoxy (DGEBA) and graphene nanoplatelets (GNP) for 0.5 hours under room temperature. A similar sonication time of 0.5 hours was also used by Surnova et al. [75] to introduce GO into epoxy resin. Mellado et al. [76] compared the exfoliation efficiencies of bath sonication (BS) and probe sonication (PS) and concluded that BS is a better technique for GO sheet synthesis. In their study Giang et al. [77] noted that BS reduced the average size of GO from 33 to 15 µm in 120 minutes. Meanwhile, PS required only 5 minutes for reducing the size of GO from 33 to 12 µm.

2.1.3 Ultrasonication- Issues

It is interesting to note that sonication for longer intervals of time could reduce agglomeration but can lead to the fragmentation of the GO sheets [66]. This observation was also supported in the study [78], which stated that a 5 hour BS could degrade the tensile strength and elastic modulus. This is possibly because, prolonged sonication can lead to an increase in temperature, which could facilitate the early polymerization of polymer chains . Moreover, sonication time can affect the defects, morphology, and interlayer spacing [79].

It has been reported that with an increase in sonication time and intensity, better dispersion of carbon nanotube (CNT) can be achieved. However, severe damage to structure (conversion of graphene layers to amorphous carbon) accompanied by a deterioration in electrical and mechanical properties was observed beyond 4 hour sonication time [80]. This observation was also supported in the study [81] which stated that the localized energy introduction in PS can lead to local heating, dislocation, bending and rupture of CNTs. It was also noted that initially, dispersion energy can cause a reduction in the size of nanoparticles, favoring dispersion. However, as time elapses, the particles tend to agglomerate leading to

a bigger size [82]. A similar trend was also reported in the dispersion of GNPs with epoxy resin [83].

Wang et al. [84] reported that ultrasonication for longer time periods decreased the electrolyte's viscosity and thermal conductivity. This is attributed to deagglomeration, shortening of particles and homogenization [85]. This was contradicted by Amrollahi et al. [86], who stated that a rise in sonication time increases the nanofiller-fluid interface leading to the formation of loose particle clusters and an increase in thermal conductivity. A consensus was formulated in the studies of Asadi et al. [87], who proposed the variation of sonication time and thermal conductivity as a bell curve with the peak at 1 hour of sonication time.

A high intensity sonication could facilitate the breakage of agglomerates into small pieces, increasing thermal contact resistance. It can also cause damages to the basal plane, consequently leading to partial removal or fragmentation of functional groups [77]. The removal of functional groups in GO with sonication was also reported in studies of Nam et al. [88]. From these studies, it is clear that there exists a critical sonication time and intensity, which has to be optimized during the processing stage.

2.1.4 Three roll milling and shear mixing

Three roll mill is a versatile machine used in different industries to produce fine particle dispersions. This is because, the high shear and compressive forces of the rollers facilitate better dispersion of agglomerates. Furthermore, it offers numerous other advantages, including narrow particle distribution, better temperature control, easy maintenance, and less contamination. The study [89] used three roll milling (TM) to peel graphene sheets of thickness 1.13 to 1.41 nm from natural graphite.

Li et al. [90] reported better exfoliation and dispersion of GNP in epoxy resin by optimizing the rotating speed and separation distance of rollers in TM. In another study, a clean and transparent solution of DGEBA clay nanoparticles was produced by conducting TM for 3 hours [91]. The thermal and electrical properties of GNP filled composites produced by

TM showed a remarkable increase compared to mechanical mixing [92]. This was further supported in the study where GNP was introduced into epoxy resin, which demonstrated that by optimizing TM, a high electrical conductivity could be achieved [93]. In their study [94] on fabricating CNT-based composites, Ha et al. observed a high degree of correlation of TM time duration with filler length and dispersion state. They reported an inverse relationship between the aspect ratio of the filler and the dispersion state. An interesting study [95] combined PS and TM in the dispersion study of nano clay particles in an epoxy matrix. However, this led to poor exfoliation, possibly due to the degradation of the polymer.

Shear mixing (SM) is a process of generating high shear forces on materials to disperse nanoparticles by breaking agglomerates [96]. The application of this process to graphene and related materials was reported in the studies of Paton et al. [97] in their research of scalable production of defect-free graphene by shear exfoliation. The study reported a critical shear rate for GNPs above which exfoliation can occur. In their research [78] to develop nanocomposites with graphite-based materials, Asma et al. concluded that BS followed by SM can improve elastic modulus and tensile strength. A similar approach was also taken in the research [59] that studied the dispersion of GO on polystyrene. BS was followed by SM for 30,60 and 60,120 minutes, respectively.

A study [98] on the introduction of GNP into epoxy composites reported that SM at 3000 rpm and 2 hours could reduce the agglomerate size by 30 percent compared to 1000 rpm and 1 hour. Moreover, there was a 12 percent increase in Young's modulus and no change in tensile strength. In another study [99] performed on nickel hydroxide-GO based composites, it was observed that SM at 3000 rpm for 15 minutes led to a low aggregation of GO.

2.1.5 Liquid phase exfoliation

Apart from exfoliation by mechanical methods, liquid phase exfoliation using solvents like DMF , N-methyl-2-pyrrolidone (NMP) can be used to create stable dispersion of GO. These organic solvents can reduce the potential energy between layers thereby helping to overcome

Van der Waals forces. They also stabilize the dispersion of GO in the SPE, since the solvent-layer interaction balances the inter layer attractive forces. However, in order to produce stable dispersion, the surface tension and solubility parameters of the solvent should be compatible with that of GO. The compatibility of a solvent with GO is often quantified using its dipole moment, Hansen solubility parameter and zeta potential values [100, 101]. Meanwhile, using solvents can often lead to low yields, difficulty in removing them, and reaggregation of particles [69].

Several studies [102, 103] have reported the critical effect of filler morphology on the development of conductive networks, and this is often quantified by IC . This is because IC in SPEs is realized by the movement of Li ion from one coordination site to another (metal ion migration) in the presence of an electric field. This requires a well dispersed amorphous polymer chain segment that facilitates Brownian motion [104].

Study [90] observed that the variation of conductivity and time duration of TM resembled a bell curve. Khan et al. [105] reported that GO lowers the percolation threshold by distributing itself along the polymer matrix leading to a decrease in contact resistance. However, this depends on how well the GO is dispersed evenly and uniformly in the matrix. The weight percent of GO in the SPE, sonication time, intensity, different processing methods and processing sequences must be studied in detail and optimized for high-quality dispersion and improved IC. The study aims to bridge this gap.

2.2 Materials, experimental setup and methodology

All chemicals were used as received unless otherwise stated. PEG with an average molecular weight of 600 and lithium salt-lithium bis(trifluoromethylsulphonyl)imide (LiTFSI) was purchased from Acros Organics® (Acros Organics, part of Thermo Fisher Scientific®, Fair Lawn,New Jersey). EPON 862 epoxy resin and EPIKURE 3274 curing agent were manufactured by Hexion™ (Hexion, Columbus, Ohio), and supplied by Miller-Stephenson™ (Miller Stephenson, Danbury, Connecticut). Graphene oxide was purchased from Nanoshel®

(Nanoshel UK, Cheshire, United Kingdom). The bath sonicator was purchased from VWR™ (Make- VWR, Model 75 D, Radnor, Pennsylvania) and the shear mixer from Ika works® (Make-Ika works Ultra Turrax® T25 Basic S1, Wilmington, North Carolina). BS was performed at power level intensities 3,6,and 9 for durations of 0.5,1,2 and 3 hours. SM was performed at 11000 rpm for 10 minutes. Three roll mill was purchased from Torrey Hills Technologies® (Make-Torrey Hills Technologies LLC, Model TM-65, San Diego, California). TM was performed 10 times. The ultrasonic immersion probe sonicator was purchased from Tekmar® (Make-Tekmar, Model TM750, Cincinnati, Ohio). The mixture was sonicated at an amplitude of 40 percent for 30, 60, and 90 minutes at a 1:2 pulse on-off ratio.

2.2.1 Electrolyte preparation

PEG was taken in a beaker and heated till it attains a liquid state. 0.5 weight percent of GO is added to PEG, and the mixture is magnetically stirred for an hour. BS, SM, TM and PS were performed to ensure uniform dispersion. Of these processes, only BS was common in all studies. Different combinations with BS, for example, BS followed by SM or TM; or PS followed by BS, were conducted to study the relative significance of each process on IC. The BS, SM,TM and PS processes are shown in figure 8. 10 weight percent lithium salt - LiTFSI was added to the PEG-GO mixture. The PEG-GO-LiTFSi mixture was magnetically stirred in an inert environment. The process continued till all the LiTFSi was dissolved. The mixture is weighed, and an equal amount of epoxy hardener in the ratio 5: 2 ratio is prepared in a separate beaker. The epoxy hardener mixture is degassed multiple times to remove any bubbles. The PEG-GO-LiTFSi mixture was added to epoxy hardener and mixed using a magnetic stirrer. The process continued until a homogeneous mixture was obtained and was followed by degassing. Finally, the electrolyte was poured into a silicon mold and subjected to curing for 24 hours at 60 °C.

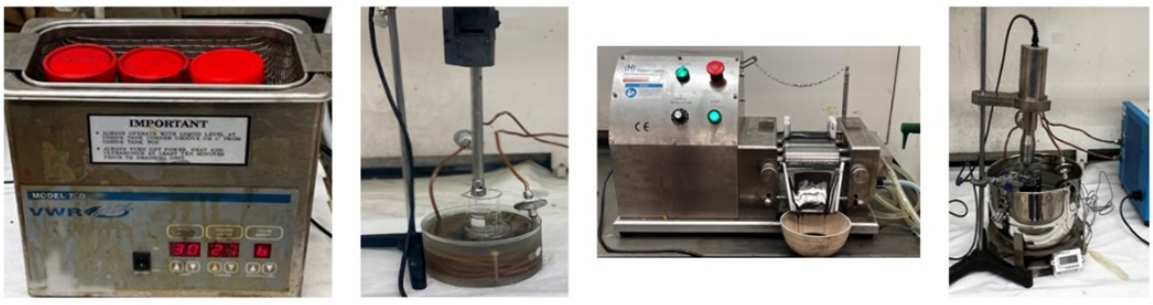

Figure 8: Processing techniques (a) bath Sonication (b) shear mixing (c) three roll milling (d) probe sonication.

2.2.2 Ionic conductivity measurement

IC at room temperature was measured using a potentiostat (Make-Princeton Applied Research ®, Versastat 3F, Ametek Scientific Instruments ®, Oak Ridge, TN). The SPE was cut into circular discs of 4 mm radius, and conductivities were measured using two outer working electrodes by sandwiching the disc between two stainless steel electrodes. The AC impedance spectroscopy was collected from 1 Hz to 1 MHz. The resistance of the SPE (R) was calculated from the intersection of the real impedance in the Nyquist plot with the semicircle fit. The through-plane conductivity (σ) was determined using the following equation.

$$\sigma = \frac{d}{R \times A} \tag{2.2.1}$$

where d and A are the thickness and area of the specimen respectively. A total of five readings were taken for each sample and the values were averaged.

2.3 Results and discussions

2.3.1 Effect of bath sonication intensities

Figure 9 and table 9 demonstrate the variation of IC for different power level intensities (3, 6, and 9) when the electrolyte was subjected to BS. Power level intensity, hereafter referred to as intensity, corresponds to the electrical energy in watts per gallon supplied to the transducers causing cavitation.

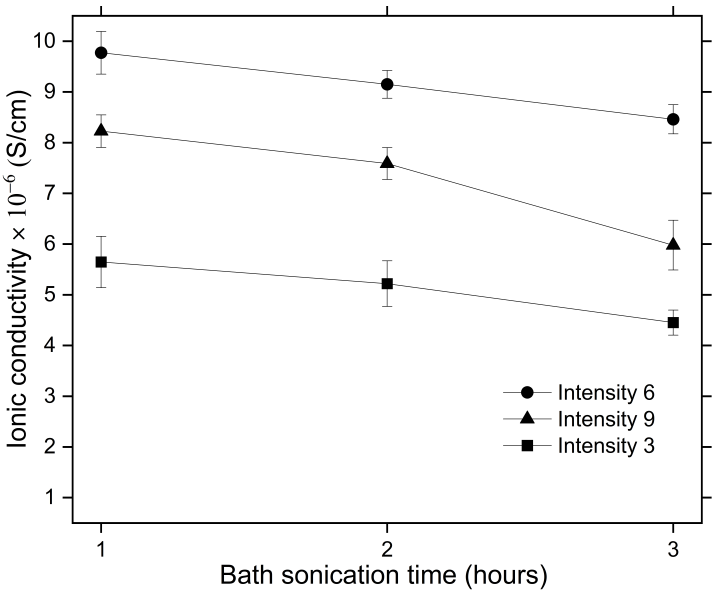

Figure 9: Variation of IC with BS at different intensities.

Intensity	Time (hour)	IC $\times 10^{-6}$(S/cm)	Reduction (%)
3	1	5.6 ± 0.5	-
3	2	5.2 ± 0.4	7.6
3	3	4.5 ± 0.2	21.2
6	1	9.8 ± 0.4	-
6	2	9.1 ± 0.3	6.4
6	3	8.5 ± 0.3	13.4
9	1	8.2 ± 0.3	-
9	2	7.6 ± 0.3	7.8
9	3	6.0 ± 0.5	27.3

Table 9: Variation of IC with BS at different intensities.

IC was highest when BS was performed at intensity 6 for an hour. This impressive value of IC at intensity 6 was 42 and 16 percent higher than at intensities 3 and 9 respectively.

It was also noted that as the duration of BS exceeds beyond one hour, there is a significant decrease in IC. All the three intensities reported over 10 percent drop in IC when BS was conducted for 3 hours.

When intensity is increased, sonication occurs more vigorously. This is because, with an increase in intensity, the power received by the transducers increases. This can be related to how much they expand and contract, which determines the power which goes to the liquid. However, an increase in intensity above a threshold limit could damage the functional groups in GO. For example, the epoxy and hydroxyl groups at the basal plane and carboxy groups at the edges are affected by high intensity. This could negatively impact the extent of dispersion as these reactive groups are primarily responsible for intercalation of GO with the polymer matrix. It is also noted that beyond one hour, IC starts decreasing. The initial increase is attributed to better dispersion. However, as the process proceeds further, the particles begin to agglomerate, increasing size and viscosity, causing a drop in IC. This bell-shaped variation between sonication time and properties is consistent with other related studies [82, 87]. The study identified 30 minutes and intensity 6 as the optimum BS parameters since they demonstrated the highest IC (Figure 10).

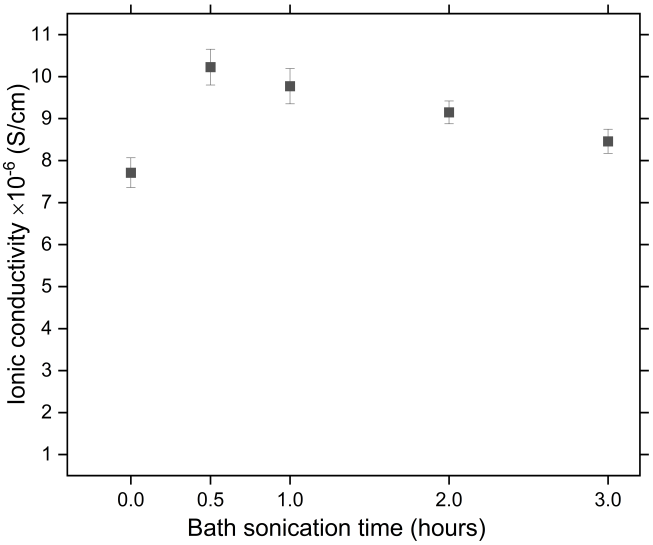

Figure 10: Variation of IC with BS time at intensity 6.

2.3.2 Effect of three roll milling and shear mixing

The variation of IC with BS time at intensity 6 is illustrated in figure 11 and table 10. The results indicate a decline in IC when BS was accompanied by SM and TM. It can also be noted that as BS time increases beyond one hour, IC decreases for all the cases. However, for SM and TM samples, this change is not high when compared to samples subjected to bath sonication only.

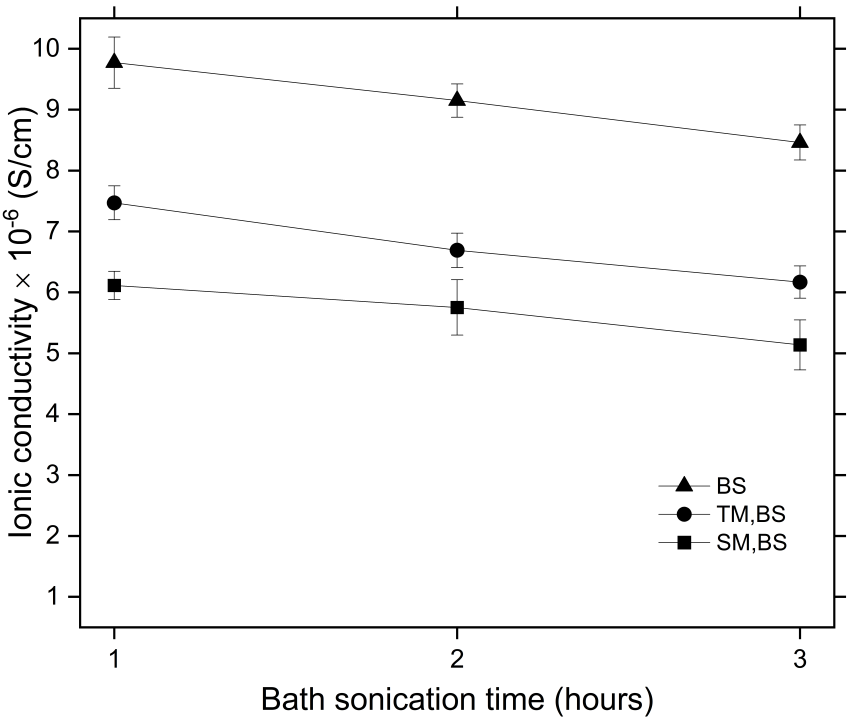

Figure 11: Variation of IC with BS at intensity 6 - with and without SM and TM.

BS time (hour)	Process	IC $\times 10^{-6}$ (S/cm)	Reduction (%)
1	BS	9.8 ± 0.4	-
1	TM, BS	7.5 ± 0.3	23.5
1	SM, BS	6.1 ± 0.2	37.5
2	BS	9.1 ± 0.3	-
2	TM,BS	6.7 ± 0.3	26.9
2	SM,BS	5.8 ± 0.5	37.2
3	BS	8.5 ± 0.3	-
3	TM,BS	6.2 ± 0.3	27.0
3	SM,BS	5.1 ± 0.4	39.2

Table 10: Variation of IC with BS at intensity 6-with and without SM and TM.

Conductivity of GO depends on many aspects, for example, the degree of exfoliation, oxidation, and presence of impurities. A fully oxidized GO has sp^3 hybridized carbon with oxygen-rich groups compared to sp^2 hybridized carbon in graphite. It has been reported [106] that any change in this structure can affect the properties of GO. For example, a fully oxidized GO acts as an insulator, while a partially oxidized one acts as a semiconductor. High speed SM or TM can damage functional groups and increase the carbon to oxygen ratio, thereby reinstating the π-π bonding between the sp^2 hybrid orbitals. Although this can help to enhance conductivity of GO, the ability of GO to intercalate with the polymer matrix is possibly affected. Furthermore, the lack of functional groups in GO can lead to an absence of a well-developed interface between GO and epoxy [98].

Parameters like the speed of SM, pressure, and shear force of the rollers in TM, and the processing time have a significant role in determining the efficacy of these processes. In addition, the probability of any reagglomeration and the relationship between the aspect ratio of GO and dispersion state after these processes has to be investigated further. Although both TM and SM were not helpful in improving the IC, the negative effect was more pronounced for SM compared to TM. This is possibly due to the high SM speed of 11000 rpm used in the study.

2.3.3 Effect of probe sonication

Figure 12 and table 11 demonstrate the change in IC when the SPE sample was subjected to PS followed by BS. PS was performed at an amplitude of 40 percent for 30, 60, and 90 minutes at a 1:2 pulse on-off ratio. BS was conducted at intensity 6 for 30 minutes in all the cases.

It can be noted that as PS time increase, IC decreases. PS was expected to outperform BS since it can provide a focused and uniform power input, considerably higher than a BS. Hence a high-quality dispersion is expected for a longer duration- high intensity PS. However, this aggressive mode of sonication can damage the functional groups, as explained in previous

sections. This is consistent with studies [76] that observed a reduction in functional groups and formation of wrinkles on GO after PS suggesting the possible degradation of morphology.

Although PS can cause local heating of the sample, it is not expected in the current study as the sample vial was placed under an ice bath. DMF was used as the solvent in PS due to its high polarity (3.82 D). Since GO contains polar oxygen functional groups like hydroxyl, carboxyl, and carbonyl, presence of a polar solvent like DMF could enhance a good GO-solvent interaction. Furthermore, the interaction between oxygen atoms in DMF and carbon atoms in GO can improve the stability of the dispersion.

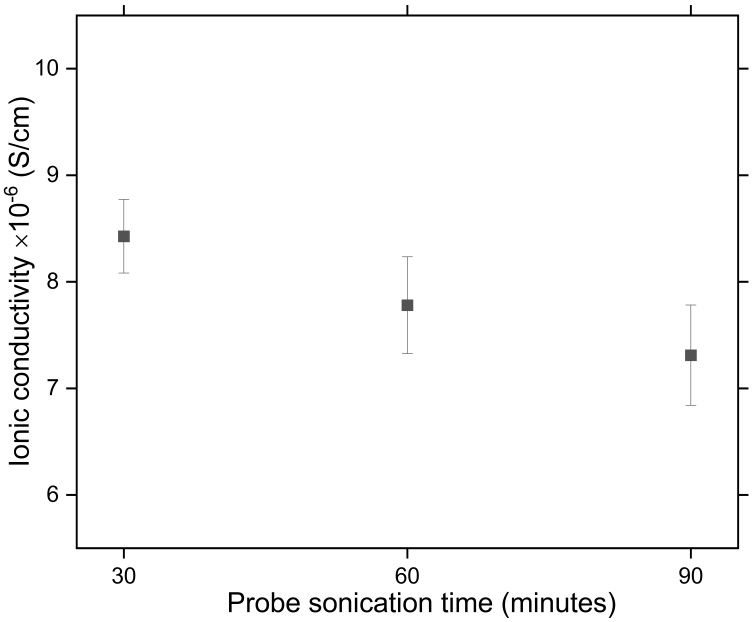

Figure 12: Variation of IC with PS time.

PS time (minutes)	IC $\times 10^{-6}$ (S/cm)	Reduction (%)
30	8.4 ± 0.3	-
60	7.8 ± 0.5	7.7
90	7.3 ± 0.5	13.3

Table 11: Variation of IC with PS time.

2.3.4 Effect of temperature and GO loading

To analyze the IC of the SPE at higher temperatures, measurements were performed between 40-70° C. Figure 13 depicts the variation of IC with temperature for different GO loadings

$(0.25 - 1.5$ weight percent).

As expected, IC increase with an increase in temperature. This is because IC in SPE occurs primarily in the amorphous region above the glass transition temperature (T_g) which facilitates better ion migration and an improved free volume distrbution. However, the effect of GO loading on IC is not linear. This is evident as a GO loading of 1 and 1.5 produced the best and worst IC. All other GO loadings were spaced between these two ranges. It can also be noted that the IC graph for GO loading 1 and 0.5 coincides initially and diverges at high temperatures. The absence of any visible surface damages or localized cracks at higher temperatures suggests the ability of the SPE to function above ambient temperature.

.

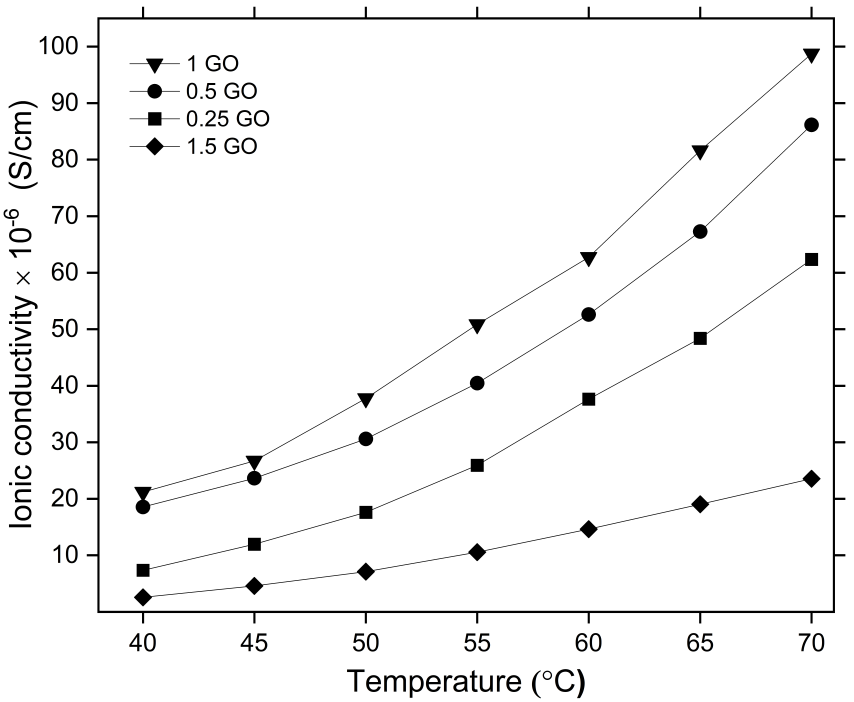

Figure 13: Variation of IC with temperature for different GO loadings $(0.25 - 1.5$ weight percent)

Figure 14 illustrates the variation in activation energy (E_A) for different GO loading. The lowest and highest E_A was reported for 0.5 and 1.5 GO loading, respectively. From the graph, it is clear that E_A of the reaction upon the addition of 0.5 to 1 percent GO is considerably

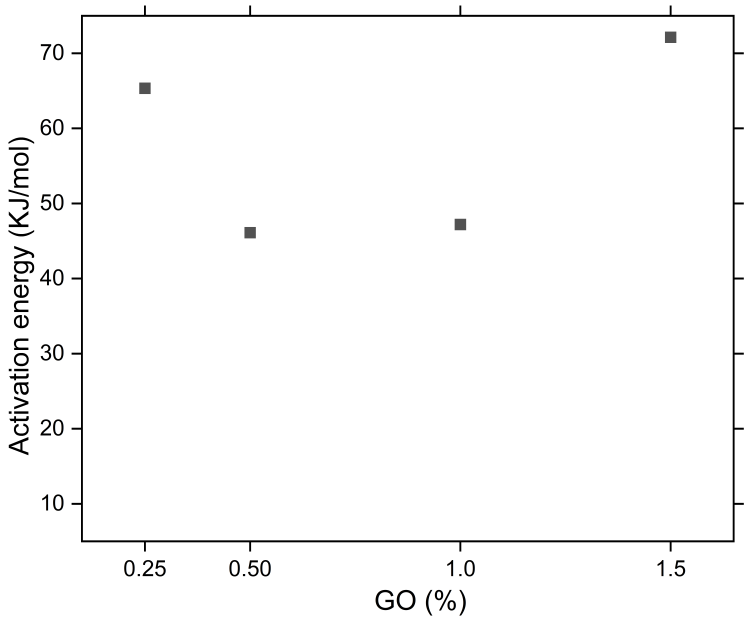

Figure 14: Variation of activation energy for different GO loading

lower than at other higher and lower weight percents. E_A is the minimum amount of energy required to start a chemical reaction; thus, it can be inferred that a system with 0.5 to 1 percent GO requires less energy to initiate. Moreover, since E_A is inversely related to the reaction rate, it is clear that 0.5-1 percent GO provides a low energy pathway for the reaction to occur, enabling the reacting particles to overcome the energy barrier easily.

2.4 Conclusion

The study presents the effects of different processing techniques like BS, PM, SM, and TM on the IC of Li-GO-PEG-Epoxy SPE. It also investigates the variation of IC with an increase in temperature and GO loading. The research proposes a clear methodology for processing SPE with respect to the technique and time duration. BS for 30 minutes at intensity 6 was found to be the optimum time and intensity for maximizing IC. There was a considerable drop in IC when the SPE was processed using SM and TM. The effect of PS on IC was also not satisfactory. This is possibly because, these processing techniques may damage the functional groups of GO and may affect its ability to intercalate to the

polymer matrix. An increase in IC with temperature is primarily attributed to an increase in the polymer chain's ionic mobility and segmental motion. The absence of any visible surface damages or localized cracks at higher temperatures suggests the ability of the SPE to function above ambient temperature. A GO weight percent of 0.5 led to a high IC and low E_A and is hence considered as an optimum weight percent in electrolyte preparation . Future investigations could include a quantitative understanding of the dispersion, agglomerations, and functional groups and studying the effect of using the SPE in making multifunctional structural supercapacitors.

CHAPTER III

EFFECT OF PEG ON THE INTERFACE PROPERTIES OF CARBON FIBER EPOXY COMPOSITES

3.1 Introduction

3.1.1 Interface and interfacial shear strength

Interface in carbon fiber reinforced polymer composites (CFRP) is the chemically bonded region that separates the matrix and the fiber surface [107]. The successful development of a mechanically efficient and durable composite system depends not just on the properties of the matrix and fiber, but also on the interface between different components. This is because in fiber reinforced polymers like CFRP, the load is transferred from the matrix to the fiber through shear. Hence a low interfacial shear strength (IFSS) can lead to less stress being transferred to the fiber, consequently creating a weaker composite with more defects and poor mechanical properties [108, 109]. Furthermore, this can also lead to a significant gap between the actual and theoretical strength of CFRP, even limiting its application to a great extent. The factors affecting the adhesion between the matrix and resin and the ensuing composite interface are well understood and has been studied as a function of interfacial shear strength.

Moosburger et al. [110] identified mechanical interlocking, physical and chemical bonding as the mechanisms responsible for adhesion between carbon fiber and polymer matrix. These are quantified by the surface roughness of the fibers and the presence of functional groups. The presence of cavities or furrows on the fiber surface can cause the polymer to be trapped

on it. Thus, rough surface morphology can often lead to better mechanical interlocking, paving the way for an improved IFSS [111]. Several studies have also reported that the presence of reactive functional groups like carboxyl, epoxy, hydroxyl, and amines on CF could improve the IFSS [112]. Apart from these factors, a higher degree of infiltration and wettability between the fiber and matrix can also enhance IFSS [113]. This is achieved by having compatible surface tension and polarity of the two phases. The mismatch of thermal expansion coefficients of the two phases can cause the development of residual stresses that can also affect the adhesion [110].

Among the different microscopic methods available for the determination of IFSS which include single fiber pull out test, single fiber push out test, microdroplet test, micro bond test etc., the single fiber fragmentation test (SFFT) is one of the most popular methods [114, 115]. In SFFT, a single fiber is extracted and placed axially on a dogbone matrix specimen. This is subjected to a tensile load. The load so applied is transferred from the matrix to the fiber through the shear stress developed at the interface, consequently elongating the fiber. This will lead to the fragmentation of the fiber and the process continues till the fibers are too short to transfer the load [116, 117, 109]. The experimental process is followed by a shear lag analysis, based on Kelly-Tyson model [118] which can be used to determine the average IFSS.

3.1.2 Studies on interfacial shear strength

Prior efforts that were aimed at improving the IFSS in CF can be broadly classified into two-oxidation and non oxidation approaches. Oxidation involves enhancing the activity of functional groups on carbon fiber (CF) surface by applying chemical oxidation agents like H_2SO_4, HNO_3, $KMnO_4$, and O_3 [119]. Non oxidation methods are generally surface modification techniques like plasma treatment, surface grafting reactions, electrolytic surface coating with epoxy,and growing carbon nanotubes (CNT) on the surface.

By oxidizing polyacrylonitrile (PAN) based CF using supercritical water and hydrogen

peroxide, Meng et.al [120] reported an increase of IFSS from 82.27 MPa to 106.66 MPa compared to untreated CF. The epoxy resin system in the study was diglycidyl-ether of bisphenol-A (DGEBA). Similar improvements were also observed in the studies of Xie et al. [121] which revealed an increase of 21 percent in IFSS when PAN based CF were subjected to atmospheric plasma treatment. The enhancement in IFSS in either case was attributed to an increase in both the oxygen rich functional groups like carboxyl and the surface roughness of the CF surface. The research [109] investigated the effect of coating multi walled CNT on CF-epoxy system and noticed an increase in IFSS. Meanwhile the ultimate tensile strength dropped by 37 percent. By adding 2 percent silica nano particles in CF-epoxy system, Liu et al. [122] succeeded in improving IFSS from 33.9 MPa to 41 MPa, an increase of 21 percent.

Studies have also compared the effect of desized (sizing removed through thermal treatment) and resized (epoxy sizing deposited) CF. It was noticed that IFSS dropped by 30 percent for desized CF [123]. It is also known that a layer of graphene oxide (GO) when deposited on the surface of CF can improve the IFSS considerably [124]. Enhancements in IFSS were also discussed in the research [125] of CF-epoxy system with 0-0.5 percent GO at low temperatures.

Fourier transform infrared spectroscopy (FTIR) and differential thermal analysis (DTA) studies by Zaverah et al. [126] on epoxy-polyethylene glycol (PEG) system with 10 percent PEG suggested that although no new functional groups are generated between epoxy and PEG, there exists a strong interaction between both. The research also identified phase separation of PEG nanoparticles in epoxy matrix and a reduction in tensile strength. Similar deductions revealing the bright PEG and dark epoxy distinct spherulite regions were also observed in the studies of Fang et al. [127] using PEG 4000-epoxy system.

3.1.3 Flexural test

One of the most widely used methods for evaluating the resistance of a specimen to bending is the flexural test. The test is also one of the macroscopic characterization methods to evaluate

interfacial bonding properties of CF [125]. The two important results of the test are flexural strength and flexural modulus. Flexural strength is the stress developed on the surface of the specimen at failure, characterized by fiber breakage. On the other hand, flexural modulus is an indication of how much a specimen can flex before attaining permanent deformation [128]. One of the unique aspects of the test is that, both tensile and compressive stresses act on the specimen, hence revealing the behavior of the laminate to these stresses [32].

The similarity of trends in the interfacial properties like interlaminar shear strength and flexural strength of CF demonstrates the close correlation of these properties. For example, Yao et al. [129] in their study of modified CF epoxy system with CNT reported that particle agglomeration and their excessive presence in the interfacial region can lead to a drop in both interlaminar shear strength and flexural strength . This observation was also supported in the study on woven CF epoxy-CNT laminates [130].

3.1.4 Studies on flexural properties

Several attempts have been made to improve the flexural properties of CF by modifying the surface by adding different materials. In the study [131], the surface of CF was modified by using GO, which resulted in an increase in flexural strength by 14 percent. The presence of functional groups in GO coupled with the high surface area of GO sheets with wrinkles improved both the chemical and mechanical interlocking between the fiber and matrix. By impregnating 10 percent PEG and silica nano particles on twill woven CF, Erdem [132] reported a considerable fall of flexural strength from 780 to 195 MPa. The flexural modulus also decreased from 35.6 to 21.6 GPa demonstrating the rapid decline in flexural properties with the addition of shear thickening fluids, caused by an enhancement in ductility.

The dependence of flexural strength of CF unsaturated polyester composite with fiber volume fraction was studied by Ganjar et.al [133]. The increase in flexural strength with fiber volume fraction (upto 40 percent) was demonstrated in this study. In their study associated with developing a structural supercapacitor with CF electrode and glass fiber

separator, Nicholas et al. [134] deposited 2 percent multiwalled CNT and evaluated the flexural properties. The maximum flexural strength increased by 27 percent (from 16.74 to 21.32 MPa), and the flexural modulus was almost constant around 3 GPa. A higher standard deviation of the data revealed the uneven deposition of multiwalled CNT.

Alok et al. [32] observed an increase of flexural strength and modulus by 20 percent with the addition of 0.4 weight percent of graphene nanoplatelets (GNP) on pan-based CF. The authors attribute this increase to the interphase being more stiffer compared to bare epoxy. The correlation of interfacial adhesion and surface properties of CF on flexural strength was also reported in the studies of Brockes et al. [135]. The higher flexural strength accompanied a lower tan δ, loss modulus and higher glass transition temperature (T_g). These findings were also supported in the studies of Avila et al. [136], who used a hybrid carbon fiber- epoxy composite system with dispersed graphene. Although a significant increase in the values of flexural modulus and strength with an increase in graphene loading (0-1.5 percent) was noted, the variation in the data sets were large. These were ascribed to graphene agglomeration and cluster formation. The addition of silane treated CNTs to CF- epoxy system improved the flexural strength and modulus by 20 and 34 percent respectively. This was due to the enhanced interfacial interactions and high dispersibility between the filler material and the fiber-matrix phase [137].

Based on the review of literature, it has become clear that most of the research on the determination of IFSS and flexural properties covered both the qualitative and quantitative aspects of carbon fibers and different resin systems. However, limited studies discuss the role played by PEG -epoxy matrix on CF and how it affects the IFSS and flexural properties. Furthermore, the correlation between IFSS and flexural strength of the composite is important to set a benchmark for improving interfaces, for instance, when fillers like GO are added. This is particularly significant in the development of structural supercapacitors for energy storage applications where bicontinuous layers are present. One such example is the development of a structural supercapacitor with a CF electrode, glass fiber separator, and

epoxy-PEG matrix, where the amount of PEG added to epoxy has to be optimized for a stronger interface without comprimising its multifunctionality. The study aims to investigate the effect of PEG on the interfacial shear strength and flexural properties of CF-epoxy systems.

3.2 Materials, experimental setup and methodology

3.2.1 Single fiber fragmentation test

3.2.1.1 Calculation of interfacial shear stress

The IFSS (τ) can be determined using the following equation [138, 109]

$$\tau = \frac{d\sigma_s}{2l_c} \tag{3.2.1}$$

where, d, σ_s, and l_c are the fiber diameter, fiber strength at critical fragment length and critical fragment length respectively.

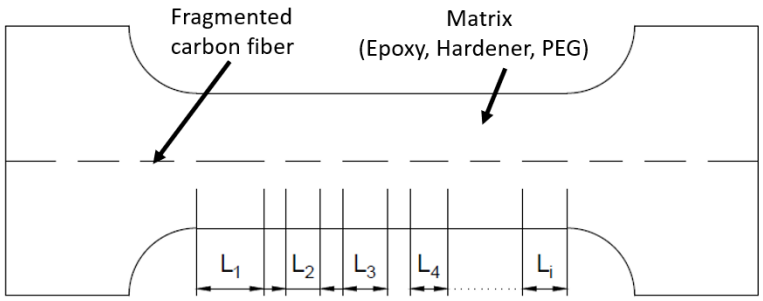

Figure 15: Schematic of the saturation of specimen after fiber breakage

Critical fiber length (l_c) is the length at which the single fiber fragments are too short for sufficient load to be transferred into them which can cause any more failure. This state is also refereed as saturation point. Most of the fiber break between $l_c/2$ and l_c. Assuming a normal distribution, the critical fragment length can be determined by taking the average fragment length ($\bar{l}$).

$$l_C = \frac{4}{3}\bar{l} \tag{3.2.2}$$

$$\bar{l} = \frac{1}{N}\sum_{i=1}^{N} l_i \tag{3.2.3}$$

Where l_i is the individual fragment length and N is the number of fragments within the gauge length (Figure 15). Since it is hard to measure the value of σ_s (due to the short fiber length), the equation to measure IFSS (τ) is modified as follows.

$$\tau = \sigma_0 \left(\frac{l_0}{\bar{l}}\right)^{\frac{1}{m}} \frac{3d}{8\bar{l}} \tag{3.2.4}$$

where σ_0, l_0 and m are the fiber strength at gauge length l_0, gauge length and Weibull shape parameter respectively.

3.2.1.2 Materials

All chemicals were used as received unless otherwise stated. PEG with an average molecular weight of 600 purchased from Acros Organics® (Acros Organics, part of Thermo Fisher Scientific®, Fair Lawn, New Jersey). EPON 862 epoxy resin and EPIKURE 3274 curing agent were manufactured by Hexion™ (Hexion, Columbus, Ohio) and supplied by Miller-Stephenson™ (Miller Stephenson, Danbury, Connecticut). CF was purchased from Fiber Glast™ (3K, 2 × 2, twill weave carbon fiber fabric, Fiber Glast. Brookville, Ohio).

3.2.1.3 Specimen preparation

The first process in specimen preparation is the extraction of a single CF. These fibers are straightened by gluing one end of the fiber and holding the other end with a light weight. Then the prestrained fiber is aligned and placed axially on the silicone mold (Figure 16). The resin is now poured into the mold. The mold is cured for 6 hours at 60° C. After curing, the specimens are removed from the mold, polished, and ensured such that the fiber is clearly

seen against the light.

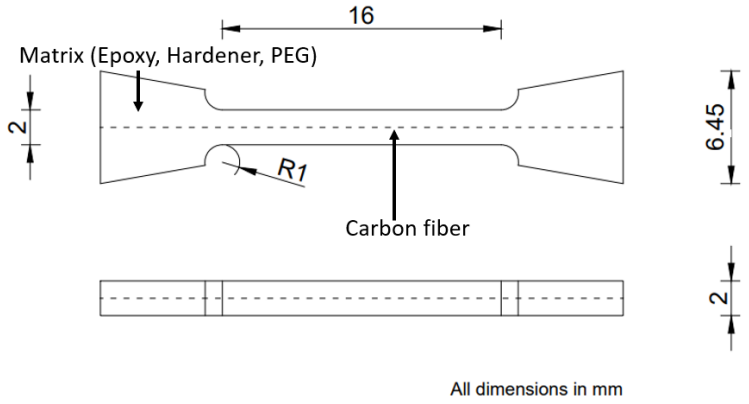

Figure 16: Silicone mold-carbon fiber embedded in matrix

3.2.1.4 Test setup

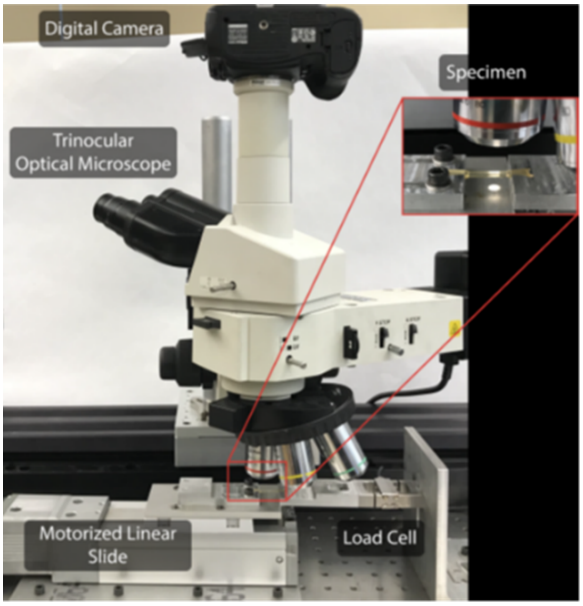

Figure 17: SFFT testing setup

Figure 17 shows the experimental setup, which is replicated from the efforts of Heckert in his study on POSS based CF [139]. When the specimen is subjected to tensile loading, the load is transferred to the CF as shear stress along the interface. With an increase in load, the fiber starts breaking, and the process continues till the generated fragments are too

small such that they cannot transfer any more load. l_c is derived from the average fragment length. The tensile strength of the fiber is determined on a tensile testing machine with a gauge length of 40.9 mm as per ASTM C1557-06 [140]. A detailed explanation of the technique can be found in the study [139].

3.2.2 Flexural strength

3.2.2.1 Calculation of flexural strength and modulus

The flexural strength and modulus were determined with a three-point bending fixture in accordance with ASTM D790 [141]. The flexural strength (σ_f) and flexural modulus (E_B) was calculated from the load (P) and support span (L) using the following equations

$$\sigma_f = \frac{3PL}{2bd^2} \tag{3.2.5}$$

$$E_B = \frac{L^3 m}{4bd^3} \tag{3.2.6}$$

where, b and d are the width and depth of the beam, respectively and m is the slope of the tangent to the initial straight-line portion of the load deflection graph. A minimum of five samples were tested for each case, and the results were averaged.

3.2.2.2 Materials

All chemicals were used as received unless otherwise stated. PEG with an average molecular weight of 600 purchased from Acros Organics® (Acros Organics, part of Thermo Fisher Scientific®, Fair Lawn, New Jersey). EPON 862 epoxy resin and EPIKURE 3274 curing agent were manufactured by Hexion™ (Hexion, Columbus, Ohio) and supplied by Miller-Stephenson™ (Miller Stephenson, Danbury, Connecticut). CF was purchased from Kynol® (ACC-5092-20 activated carbon fabric , Kynol Europa GmbH, Hamburg, Germany).

3.2.2.3 Specimen preparation

Vacuum assisted resin transfer molding (VARTM) was used to make the composite laminate. VARTM is a closed mold technique that can produce high performance polymer composites at a low cost. It uses a glass base, peel cloth, distributer mesh, vacuum bag, vacuum pump, tacky tape, resin trap, resin cup, connector plugs, and tubing. The process begins with a hand layup of four plies of carbon fibers cut in the required dimensions The layup is placed in the center of the glass plate. A layer of parting wax separates the glass base and the layup. The wax also aids in the easy release of the composite plate after the process. The epoxy resin and the hardener were prepared in the ratio of 5: 2. PEG was added to this mixture. The mixture was stirred well for homogeneity. This was further degassed multiple cycles to remove any air bubbles.

A layer of peel cloth followed by another layer of distributer mesh is placed on top of the layup. The peel cloth helps to remove the panel from the distribution medium. The distributer mesh enables easy transport of resin. The connector plugs are placed above the mesh and sealed on the glass plate using tapes. The entire arrangement is encapsulated on a vacuum bagging. Two flexible tubings are inserted into the connector plugs through the vacuum bagging. They are connected to the resin beaker and vacuum pump. The vacuum bag is sealed firmly using tacky tapes. A uniform vacuum has to be maintained throughout the experiment; hence any air leaks should be prevented to ensure a good vacuum seal.

After the vacuum bag is completely sealed, the resin is injected into the connector plug. Since the resin cup is open to the atmosphere, a differential pressure is developed between the inlet and exit regions. The flow of resin is continued until the whole of the layup is soaked in the resin. Once the layup is impregnated with the resin, the vacuum line is shut off. The vacuum pump is kept on for three more hours to ensure no more air bubbles get trapped in the resin ejection line. The composite panel is released from the glass plate and is taken for curing. Curing is done for 10 hours at 60°C. A detailed description of the VARTM process can be found in the study [142].

3.2.2.4 Test setup

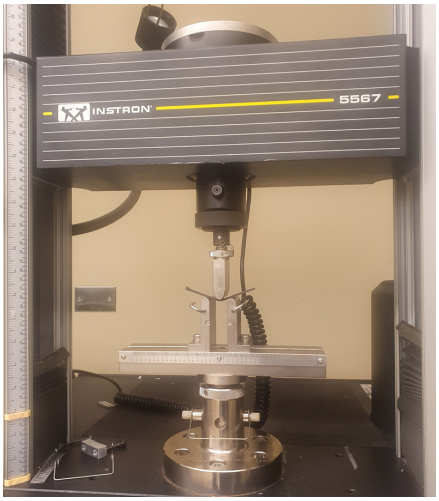

Figure 18: Flexural testing setup

After the laminate was cured, rectangular samples were cut from it following the specifications described in ASTM D790. These specimens were loaded on a flexural testing machine at three points (Make-5567, Instron Corporation, Norwood, Massachusetts). Figure 18 shows the testing set up. The specimen span to depth ratio is set as 16:1 so as to eliminate the development of high shear stress [143]. The rate of crosshead motion was set in accordance with ASTM D790 by considering the span and depth of each specimen. The application of the load leads to the bending of the specimen. This is associated with the development of compressive and tensile strains on the concave and convex sides.

3.3 Results and Discussion

3.3.1 Effect of PEG on IFSS

Table 12 demonstrate the variation in critical fiber length and average IFSS when different amount of PEG (0-5 percent) was added to the epoxy hardener. From the table, it is clear that the critical fiber length shows a significant increase when PEG is added to the epoxy hardener. Since critical fiber length is inversely related to IFSS, the change in IFSS is the opposite of this trend. The variation of average IFSS with PEG is illustrated in figure 19.

PEG (%)	Critical fiber length (μm)	Increment (%)	Avg IFSS (MPa)	Reduction (%)
0	473 ± 13	-	58	-
1	582 ± 15	23	45	22
2	630 ± 13	33	41	29
3	678 ± 11	43	38	35
4	717 ± 11	52	35	40
5	750 ± 16	54	33	43

Table 12: Variation of critical fiber length with addition of PEG

The introduction of PEG makes the matrix more ductile. In other words, when PEG is added to epoxy, a transition from the brittle to ductile character occurs. Furthermore, PEG is uniformly distributed in the epoxy matrix. This is particularly important as most of the other fillers like GO, when added to the epoxy matrix, cause uneven dispersion, and are hence subjected to cycles of sonication and often shear mixing or three roll mill to achieve quality dispersion. Moreover, the strong interaction between PEG and epoxy, as suggested in several studies [126], reveals their strong compatibility with each other.

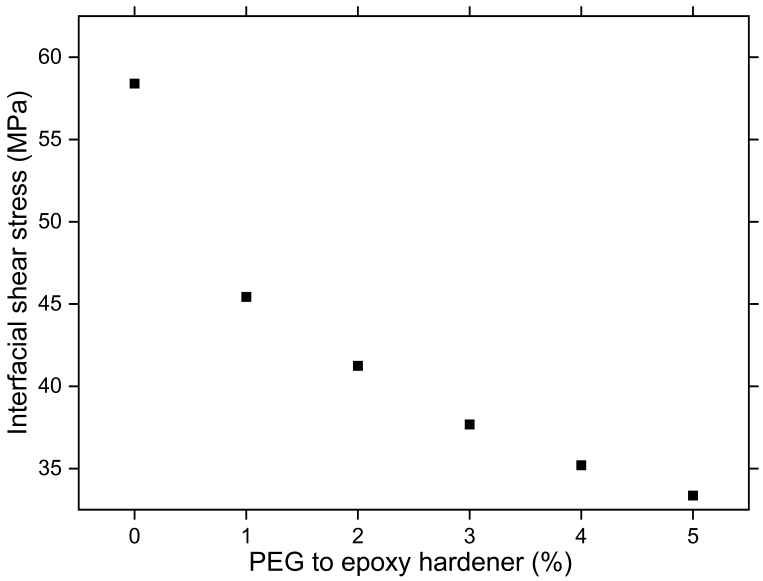

Figure 19: Variation of IFSS with addition of PEG

The superior miscibility of PEG with epoxy can also affect the cross linking density of the epoxy with the hardener. The reaction between epoxy and hardener is best described by cross linking process, causing the formation of a thermoset form. This involves the reaction

of an epoxy group with an amine hydrogen, leading to the generation of a hydroxyl group when an epoxy group is opened. This process continues, making a long chain of molecules that crosslinks, consequently enhancing the viscosity. The number of effective crosslinks per unit volume is measured by the cross link density. This normal scenario is altered by the addition of PEG, which has strong miscibility and interaction with epoxy. The higher mobility and diffusion characteristics of PEG can cause its hydroxyl end groups to react with the epoxy groups, for example, infiltrating the polymer chain and spacing them apart. This can lead to a lower crosslinking density, characterized by a change from a rigid to a flexible structure. This ductile character accounts for the increase in critical fiber length and explains why the SFFT is not suitable for higher PEG loadings.

Although the rate of the reaction between PEG and epoxy is slower than the rate between the epoxy and the amine hydrogen, it is expected that a considerable amount of this reaction can occur, especially if the hardener is the limiting reactant. This is evident from the decreased T_g of the polymer. T_g is the temperature at which the polymer undergoes a transition from a rigid to a more flexible (rubbery) state. The decrease in T_g with an addition of PEG to epoxy can also be observed from the Fox equation graph of the epoxy-PEG mixture (Figure 20). The T_g for pure epoxy and pure PEG is taken as 107 and -41 °C, respectively. It is interesting to note that the addition of just 5 percent of PEG led to the decrease in T_g by 11 percent, signifying the considerable difference in the T_g of pure epoxy and pure PEG. A low T_g enables the polymer chain to move easily and generate more free volume. On the other hand, a high T_g implies a stiff and rigid molecular structure.

Apart from the effects of PEG addition on epoxy discussed above, it can also alter the fiber-matrix interface. Since PEG forms a nano blend morphology in the epoxy matrix [126], it can increase the interfacial area, consequently facilitating a high degree of interaction with the epoxy matrix at the interface. The interfacial adhesion of the CF with epoxy alone is considerably higher than with an epoxy-PEG mixture. This is primarily attributed to the plasticizing effect of PEG coupled with the low viscosity of the epoxy-PEG mixture.

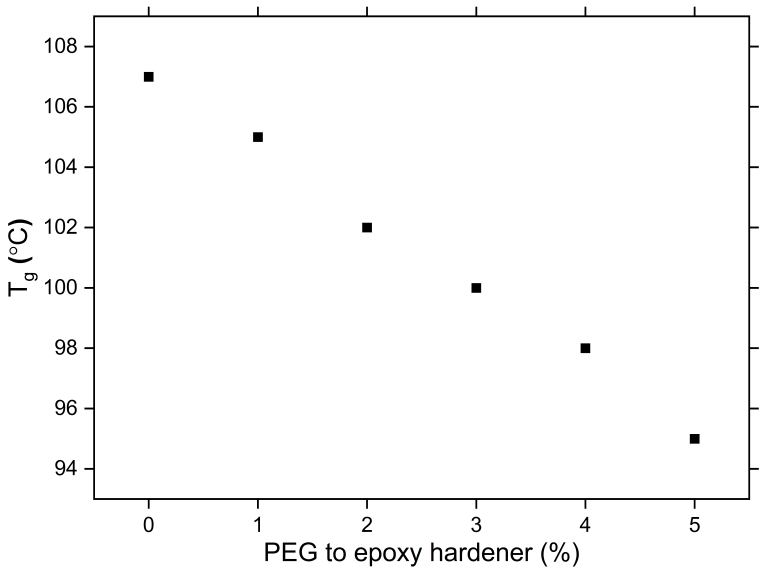

Figure 20: Variation of T_g with addition of PEG

Initially, PEG is expected to affect the crosslinking density of epoxy. Further, the addition of PEG along with the unreacted hardener dominates the interface region, leading to a drastic decline in IFSS. These observations are also consistent with other studies related to PEG [126, 144, 145].

3.3.2 Effect of PEG on flexural properties

Flexural test was conducted to study the effect of adding PEG to epoxy at higher weight percentages (0-50 percent). Figure 21 and 22 demonstrate the variation of flexural strength and flexural modulus when different amount of PEG (0-50 percent) was added to the epoxy hardener mixture. The corresponding values are shown in tables 13 and 14.

PEG (%)	Flexural strength (MPa)	Reduction (%)
0	55.4 ± 1.3	-
10	23.7 ± 1.7	57.2
20	15.9 ± 1.2	71.4
30	11.4 ± 1.1	79.4
40	5.7 ± 0.7	89.7
50	3.2 ± 0.2	94.3

Table 13: Variation of flexural strength with addition of PEG

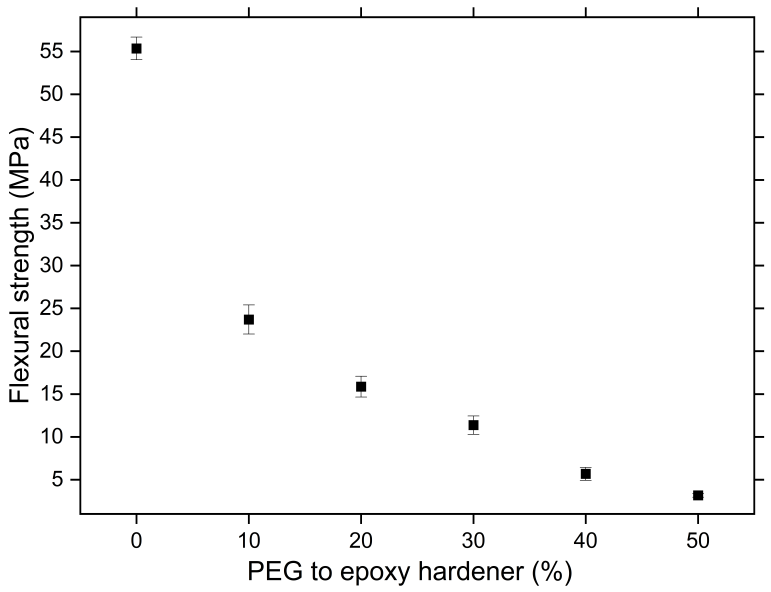

Figure 21: Variation of flexural strength with addition of PEG

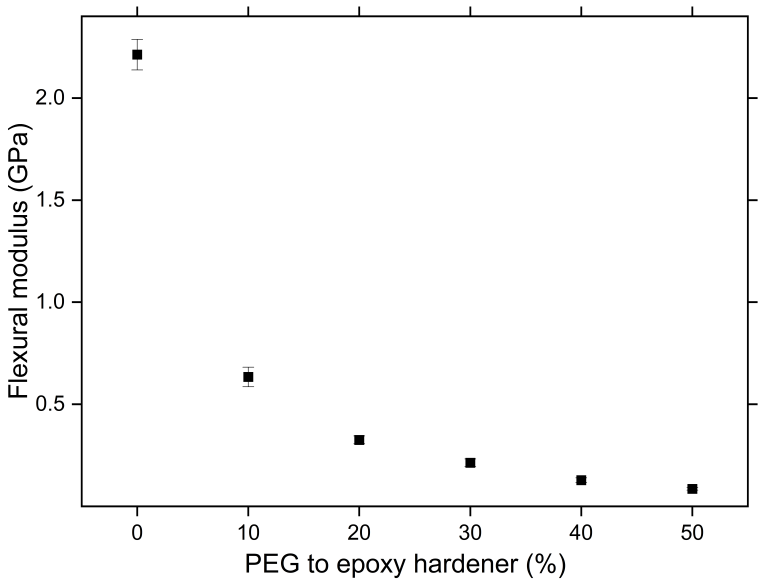

Figure 22: Variation of flexural modulus with addition of PEG

PEG (%)	Flexural modulus (GPa)	Reduction (%)
0	2.21 ± 0.07	-
10	0.63 ± 0.05	71.50
20	0.33 ± 0.02	85.06
30	0.21 ± 0.02	90.50
40	0.13 ± 0.01	94.11
50	0.09 ± 0.01	95.93

Table 14: Variation of flexural modulus with addition of PEG

From the graph, it is clear that there is a significant reduction in flexural strength (57.17 percent) when 10 percent PEG is added to the epoxy hardener. Furthermore, the flexural strength decreases steeply with further addition of PEG, reaching a massive drop of 94 percent for 50 percent addition. Similar trends were also observed for flexural modulus. The 72 percent drop in flexural modulus with a 10 percent addition of PEG is evident from the graph. The sharp decline of flexural modulus continues with further loading of PEG, reaching a decrease of 96 percent for 50 percent PEG. From the results it is clear that addition of PEG could significantly affect the flexural strength.

The flexural properties primarily depend on fiber-matrix interfacial strength and matrix properties. The absence of any functionalization on CFs in the study eliminates the possibility of having groups like amide, carboxyl etc. which could chemically react with unreacted hardener through covalent or hydrogen bonds. Moreover, the oxygen and nitrogen concentrations on the fiber surface should be negligible since the fibers were untreated. These factors can considerably reduce the extent of chemical bonding and CF surface wettability.

A system with CF and epoxy alone has higher flexural properties due to good dispersibility and improved interfacial interactions facilitating homogenous load support of the fibers. However, adding PEG to epoxy can lead to softening of the matrix, as discussed in previous sections. This could affect the surface profile and roughness of the fiber, leading to poor mechanical interlocking at the interface.

Furthermore, the PEG and unreacted hardener can fill the microcavities of the composite and may lead to the development of microcracks. It can be further enhanced by the formation of agglomerates which can act as stress raisers, subsequently leading to the development of voids in the matrix. This may cause premature matrix failure, causing a drop in flexural strength. However, the probability of this occurring is significantly less compared to polymer systems with fillers like GO, where perfect dispersion is often hard to achieve.

Thus, addition of PEG coupled with the absence of any functionalization of the CF surface, minimizes mechanical interlocking, chemical bonding and CF surface wettability.

Since these factors are critical for a stronger interface, it can be concluded that the interface is weak. This is also supported by the SFFT studies on epoxy-PEG system discussed before. The delamination between the fiber and epoxy was evident in the study, which further demonstrates a weak interfacial bonding. A thick interphase leads to a higher bending strength due to improved load transfer between the fiber and matrix. Hence, even if the modulus and strength is very high along the uniaxial direction, the specimen could fail easily when subjected to flexural loading due to the weak interface between the fiber and matrix.

3.4 Conclusion

The study presents the mechanical properties (IFSS and flexural properties) of carbon fiber epoxy laminates with different weight percentages of PEG. IFSS and flexural properties were determined using SFFT and three point bending test, respectively. The decline in IFSS is primarily attributed to the changes in fiber- matrix interface caused by the addition of PEG. The miscibility between PEG and epoxy was found to be high, and the addition of PEG affects the crosslinking density of the matrix. This is due to its higher mobility and diffusion characteristics. Moreover, adding PEG to epoxy led to a decline in the T_g of the matrix. The plasticizing effect of PEG, which in turn made the matrix ductile posed serious challenges to extending SFFT beyond 5 percent of PEG loading. The absence of functionalization on the CF surface and the negligible concentrations of oxygen and nitrogen reduces the extent of chemical bonding at the interface. In addition to this, the low viscous PEG and hardener can fill microcavities affecting the mechanical interlocking and surface roughness. These factors can further lead to a weak interface facilitating interfacial debonding and a decline in flexural properties. The correlation in the trends of IFSS and flexural properties on PEG loading was identified, and it was observed that both the properties show similar trends on adding PEG. Future investigations could include the quantitative understanding of the interphase width and constituents, and studying the effect of fillers like GO on epoxy-PEG resin system.

REFERENCES

[1] J. Gou, Y. Tang, F. Liang, Z. Zhao, D. Firsich, and J. Fielding, "Carbon nanofiber paper for lightning strike protection of composite materials," *Composites Part B: Engineering*, vol. 41, no. 2, pp. 192–198, 2010.

[2] A. Larsson, "The interaction between a lightning flash and an aircraft in flight," *Comptes Rendus Physique*, vol. 3, no. 10, pp. 1423–1444, 2002.

[3] S. T. Kotikalapudi, R. Akula, and R. P. Singh, "Degradation mechanisms in carbon fiber–epoxy laminates subjected to constant low-density direct current," *Composites Part B: Engineering*, vol. 233, p. 109516, 2022.

[4] M. Gagné and D. Therriault, "Lightning strike protection of composites," *Progress in Aerospace Sciences*, vol. 64, pp. 1–16, 2014.

[5] S. Mall, B. Ouper, and J. Fielding, "Compression strength degradation of nanocomposites after lightning strike," *Journal of composite materials*, vol. 43, no. 24, pp. 2987–3001, 2009.

[6] F. A. Fisher and J. A. Plumer, "Lightning protection of aircraft," tech. rep., 1977.

[7] D.-C. Seo and J.-J. Lee, "Damage detection of cfrp laminates using electrical resistance measurement and neural network," *Composite structures*, vol. 47, no. 1-4, pp. 525–530, 1999.

[8] P. Irving and C. Thiagarajan, "Fatigue damage characterization in carbon fibre composite materials using an electrical potential technique," *Smart materials and structures*, vol. 7, no. 4, p. 456, 1998.

[9] R. Hart and O. Zhupanska, "Characterization of carbon fiber polymer matrix composites subjected to simultaneous application of electric current pulse and low velocity impact," in *53rd AIAA/ASME/ASCE/AHS/ASC Structures, Structural Dynamics and Materials Conference 20th AIAA/ASME/AHS Adaptive Structures Conference 14th AIAA*, p. 1381, 2011.

[10] M. F. Haider, P. K. Majumdar, S. Angeloni, and K. L. Reifsnider, "Nonlinear anisotropic electrical response of carbon fiber-reinforced polymer composites," *Journal of composite materials*, vol. 52, no. 8, pp. 1017–1032, 2018.

[11] S. Dong and R. Gauvin, "Application of dynamic mechanical analysis for the study of the interfacial region in carbon fiber/epoxy composite materials," *Polymer composites*, vol. 14, no. 5, pp. 414–420, 1993.

[12] B. Ray, "Temperature effect during humid ageing on interfaces of glass and carbon fibers reinforced epoxy composites," *Journal of colloid and interface science*, vol. 298, no. 1, pp. 111–117, 2006.

[13] M. Ieda, "Dielectric breakdown process of polymers," *IEEE Transactions on Electrical Insulation*, no. 3, pp. 206–224, 1980.

[14] Z. Jia, T. Li, F.-p. Chiang, and L. Wang, "An experimental investigation of the temperature effect on the mechanics of carbon fiber reinforced polymer composites," *Composites Science and Technology*, vol. 154, pp. 53–63, 2018.

[15] G. Odegard and M. Kumosa, "Elastic-plastic and failure properties of a unidirectional carbon/pmr-15 composite at room and elevated temperatures," *Composites Science and Technology*, vol. 60, no. 16, pp. 2979–2988, 2000.

[16] S. Cao, X. Wang, and Z. Wu, "Evaluation and prediction of temperature-dependent tensile strength of unidirectional carbon fiber-reinforced polymer composites," *Journal of Reinforced Plastics and Composites*, vol. 30, no. 9, pp. 799–807, 2011.

[17] G. Aklilu, S. Adali, and G. Bright, "Temperature effect on mechanical properties of carbon, glass and hybrid polymer composite specimens," in *International Journal of Engineering Research in Africa*, vol. 39, pp. 119–138, Trans Tech Publ, 2018.

[18] K. Chung, J. Seferis, and J.-D. Nam, "Investigation of thermal degradation behavior of polymeric composites: prediction of thermal cycling effect from isothermal data," *Composites Part A: Applied Science and Manufacturing*, vol. 31, no. 9, pp. 945–957, 2000.

[19] S. T. Kotikalapudi and R. P. Singh, "Mechanical strength degradation of carbon fiber polymer matrix composites exposed to constant low-density direct current," in *ASME International Mechanical Engineering Congress and Exposition*, vol. 59490, p. V012T10A052, American Society of Mechanical Engineers, 2019.

[20] H. Kaftelen-Odabaşı, A. Odabaşı, M. Özdemir, and M. Baydoğan, "A study on graphene reinforced carbon fiber epoxy composites: Investigation of electrical, flexural, and dynamic mechanical properties," *Polymer Composites*.

[21] B. O. Lee, W. J. Woo, and M.-S. Kim, "Emi shielding effectiveness of carbon nanofiber filled poly (vinyl alcohol) coating materials," *Macromolecular Materials and Engineering*, vol. 286, no. 2, pp. 114–118, 2001.

[22] S. Xie, Y. Liu, and J. Li, "Comparison of the effective conductivity between composites reinforced by graphene nanosheets and carbon nanotubes," *Applied Physics Letters*, vol. 92, no. 24, p. 243121, 2008.

[23] A. Alan, S. T. Kotikalapudi, and R. P. Singh, "How graphene oxide content in poly (ethylene glycol) affects phase separation in epoxy matrix for high-performance structural supercapacitor applications," in *Conference Proceedings of the Society for Experimental Mechanics Series,*, Society for Experimental Mechanics.

[24] P.-C. Ma, N. A. Siddiqui, G. Marom, and J.-K. Kim, "Dispersion and functionalization of carbon nanotubes for polymer-based nanocomposites: A review," *Composites Part A: Applied Science and Manufacturing*, vol. 41, no. 10, pp. 1345–1367, 2010.

[25] S.-Y. Yang, C.-C. M. Ma, C.-C. Teng, Y.-W. Huang, S.-H. Liao, Y.-L. Huang, H.-W. Tien, T.-M. Lee, and K.-C. Chiou, "Effect of functionalized carbon nanotubes on the thermal conductivity of epoxy composites," *Carbon*, vol. 48, no. 3, pp. 592–603, 2010.

[26] N. Mehra, L. Mu, T. Ji, X. Yang, J. Kong, J. Gu, and J. Zhu, "Thermal transport in polymeric materials and across composite interfaces," *Applied Materials Today*, vol. 12, pp. 92–130, 2018.

[27] K. A. Imran and K. N. Shivakumar, "Enhancement of electrical conductivity of epoxy using graphene and determination of their thermo-mechanical properties," *Journal of Reinforced Plastics and Composites*, vol. 37, no. 2, pp. 118–133, 2018.

[28] J. A. King, D. R. Klimek, I. Miskioglu, and G. M. Odegard, "Mechanical properties of graphene nanoplatelet/epoxy composites," *Journal of applied polymer science*, vol. 128, no. 6, pp. 4217–4223, 2013.

[29] H. Fukushima, *Graphite nanoreinforcements in polymer nanocomposites*. Michigan State University, 2003.

[30] M. A. Rafiee, J. Rafiee, Z. Wang, H. Song, Z.-Z. Yu, and N. Koratkar, "Enhanced mechanical properties of nanocomposites at low graphene content," *ACS nano*, vol. 3, no. 12, pp. 3884–3890, 2009.

[31] S. Chatterjee, F. Nafezarefi, N. Tai, L. Schlagenhauf, F. Nüesch, and B. Chu, "Size and synergy effects of nanofiller hybrids including graphene nanoplatelets and carbon nanotubes in mechanical properties of epoxy composites," *Carbon*, vol. 50, no. 15, pp. 5380–5386, 2012.

[32] A. K. Srivastava, V. Gupta, C. S. Yerramalli, and A. Singh, "Flexural strength enhancement in carbon-fiber epoxy composites through graphene nano-platelets coating on fibers," *Composites Part B: Engineering*, vol. 179, p. 107539, 2019.

[33] J. Cho, J. Chen, and I. Daniel, "Mechanical enhancement of carbon fiber/epoxy composites by graphite nanoplatelet reinforcement," *Scripta materialia*, vol. 56, no. 8, pp. 685–688, 2007.

[34] F. Yavari, M. Rafiee, J. Rafiee, Z.-Z. Yu, and N. Koratkar, "Dramatic increase in fatigue life in hierarchical graphene composites," *ACS applied materials & interfaces*, vol. 2, no. 10, pp. 2738–2743, 2010.

[35] Y. Zhang, Y. Wang, J. Yu, L. Chen, J. Zhu, and Z. Hu, "Tuning the interface of graphene platelets/epoxy composites by the covalent grafting of polybenzimidazole," *Polymer*, vol. 55, no. 19, pp. 4990–5000, 2014.

[36] R. Atif, I. Shyha, and F. Inam, "Mechanical, thermal, and electrical properties of graphene-epoxy nanocomposites—a review," *Polymers*, vol. 8, no. 8, p. 281, 2016.

[37] D. Wentzel, S. Miller, and I. Sevostianov, "Dependence of the electrical conductivity of graphene reinforced epoxy resin on the stress level," *International Journal of Engineering Science*, vol. 120, pp. 63–70, 2017.

[38] H. Kim, A. A. Abdala, and C. W. Macosko, "Graphene/polymer nanocomposites," *Macromolecules*, vol. 43, no. 16, pp. 6515–6530, 2010.

[39] S. Mann, R. Kumar, and V. Jindal, "Negative thermal expansion of pure and doped graphene," *RSC advances*, vol. 7, no. 36, pp. 22378–22387, 2017.

[40] A. K. Roy, B. L. Farmer, V. Varshney, S. Sihn, J. Lee, and S. Ganguli, "Importance of interfaces in governing thermal transport in composite materials: modeling and

experimental perspectives," *ACS applied materials & interfaces*, vol. 4, no. 2, pp. 545–563, 2012.

[41] S. Han, Q. Meng, S. Araby, T. Liu, and M. Demiral, "Mechanical and electrical properties of graphene and carbon nanotube reinforced epoxy adhesives: Experimental and numerical analysis," *Composites Part A: Applied Science and Manufacturing*, vol. 120, pp. 116–126, 2019.

[42] B. Debelak and K. Lafdi, "Use of exfoliated graphite filler to enhance polymer physical properties," *Carbon*, vol. 45, no. 9, pp. 1727–1734, 2007.

[43] F. Kargar, Z. Barani, R. Salgado, B. Debnath, J. S. Lewis, E. Aytan, R. K. Lake, and A. A. Balandin, "Thermal percolation threshold and thermal properties of composites with high loading of graphene and boron nitride fillers," *ACS applied materials & interfaces*, vol. 10, no. 43, pp. 37555–37565, 2018.

[44] M. Shtein, R. Nadiv, M. Buzaglo, K. Kahil, and O. Regev, "Thermally conductive graphene-polymer composites: size, percolation, and synergy effects," *Chemistry of Materials*, vol. 27, no. 6, pp. 2100–2106, 2015.

[45] J. Li, M. L. Sham, J.-K. Kim, and G. Marom, "Morphology and properties of uv/ozone treated graphite nanoplatelet/epoxy nanocomposites," *Composites Science and Technology*, vol. 67, no. 2, pp. 296–305, 2007.

[46] Y. Chekanov, R. Ohnogi, S. Asai, and M. Sumita, "Electrical properties of epoxy resin filled with carbon fibers," *Journal of materials science*, vol. 34, no. 22, pp. 5589–5592, 1999.

[47] R. Taherian, "Experimental and analytical model for the electrical conductivity of polymer-based nanocomposites," *Composites Science and Technology*, vol. 123, pp. 17–31, 2016.

[48] S. Tamayo-Vegas, A. Muhsan, C. Liu, M. Tarfaoui, and K. Lafdi, "The effect of agglomeration on the electrical and mechanical properties of polymer matrix nanocomposites reinforced with carbon nanotubes," *Polymers*, vol. 14, no. 9, p. 1842, 2022.

[49] H. Kaftelen-Odabaşı, A. Odabaşı, M. Özdemir, and M. Baydoğan, "A study on graphene reinforced carbon fiber epoxy composites: Investigation of electrical, flexural, and dynamic mechanical properties," *Polymer Composites*, 2022.

[50] A. S. Wajid, H. T. Ahmed, S. Das, F. Irin, A. F. Jankowski, and M. J. Green, "High-performance pristine graphene/epoxy composites with enhanced mechanical and electrical properties," *Macromolecular Materials and engineering*, vol. 298, no. 3, pp. 339–347, 2013.

[51] A. J. Marsden, D. Papageorgiou, C. Valles, A. Liscio, V. Palermo, M. Bissett, R. Young, and I. Kinloch, "Electrical percolation in graphene–polymer composites," *2D Materials*, vol. 5, no. 3, p. 032003, 2018.

[52] K. Chung, J. Seferis, and J.-D. Nam, "Investigation of thermal degradation behavior of polymeric composites: prediction of thermal cycling effect from isothermal data," *Composites Part A: Applied Science and Manufacturing*, vol. 31, no. 9, pp. 945–957, 2000.

[53] L. Vouyovitch, N. Alberola, L. Flandin, A. Beroual, and J.-L. Bessede, "Dielectric breakdown of epoxy-based composites: relative influence of physical and chemical aging," *IEEE Transactions on Dielectrics and Electrical Insulation*, vol. 13, no. 2, pp. 282–292, 2006.

[54] E. Botelho, L. Pardini, and M. Rezende, "Hygrothermal effects on the shear properties of carbon fiber/epoxy composites," *Journal of Materials Science*, vol. 41, no. 21, pp. 7111–7118, 2006.

[55] J. Suñé, N. Raghavan, and K. Pey, "Dielectric breakdown processes," *Resistive Switching: From Fundamentals of Nanoionic Redox Processes to Memristive Device Applications*, pp. 225–252, 2016.

[56] Y. Chekanov, R. Ohnogi, S. Asai, and M. Sumita, "Electrical properties of epoxy resin filled with carbon fibers," *Journal of materials science*, vol. 34, no. 22, pp. 5589–5592, 1999.

[57] S. T. Kotikalapudi and R. P. Singh, "In situ measurement of ac conductivity to quantify unidirectional alignment of graphene nanoplatelets (gnps) in epoxy," in *Conference Proceedings of the Society for Experimental Mechanics Series,*, Society for Experimental Mechanics.

[58] F. Ye, K. Liao, R. Ran, and Z. Shao, "Recent advances in filler engineering of polymer electrolytes for solid-state li-ion batteries: a review," *Energy & Fuels*, vol. 34, no. 8, pp. 9189–9207, 2020.

[59] Z. G. Mohammadsalih, B. J. Inkson, and B. Chen, "The effect of dispersion condition on the structure and properties of polystyrene/graphene oxide nanocomposites," *Polymer Composites*, vol. 42, no. 1, pp. 320–328, 2021.

[60] V. K. Thakur, G. Ding, J. Ma, P. S. Lee, and X. Lu, "Hybrid materials and polymer electrolytes for electrochromic device applications," *Advanced materials*, vol. 24, no. 30, pp. 4071–4096, 2012.

[61] S. Stankovich, D. A. Dikin, G. H. Dommett, K. M. Kohlhaas, E. J. Zimney, E. A. Stach, R. D. Piner, S. T. Nguyen, and R. S. Ruoff, "Graphene-based composite materials," *nature*, vol. 442, no. 7100, pp. 282–286, 2006.

[62] X. Wang, J. Jin, and M. Song, "An investigation of the mechanism of graphene toughening epoxy," *Carbon*, vol. 65, pp. 324–333, 2013.

[63] Y. J. Wan, L. X. Gong, L. C. Tang, L. B. Wu, and J. X. Jiang, "Mechanical properties of epoxy composites filled with silane-functionalized graphene oxide," *Composites Part A: Applied Science and Manufacturing*, vol. 64, pp. 79–89, 2014.

[64] J. Cao, G. Q. Qi, K. Ke, Y. Luo, W. Yang, B. H. Xie, and M. B. Yang, "Effect of temperature and time on the exfoliation and de-oxygenation of graphite oxide by thermal reduction," *Journal of Materials Science*, vol. 47, no. 13, pp. 5097–5105, 2012.

[65] H. Chen, M. B. Müller, K. J. Gilmore, G. G. Wallace, and D. Li, "Mechanically strong, electrically conductive, and biocompatible graphene paper," *Advanced Materials*, vol. 20, no. 18, pp. 3557–3561, 2008.

[66] Y. Tian, Y. Cao, Y. Wang, W. Yang, and J. Feng, "Realizing ultrahigh modulus and high strength of macroscopic graphene oxide papers through crosslinking of mussel-inspired polymers," *Advanced materials*, vol. 25, no. 21, pp. 2980–2983, 2013.

[67] L. J. Cote, F. Kim, and J. Huang, "Langmuir- blodgett assembly of graphite oxide single layers," *Journal of the American Chemical Society*, vol. 131, no. 3, pp. 1043–1049, 2009.

[68] I. Ibrahim and M. Rummeli, "Graphene: Fundamentals and emergent applications/chapter 4 methods for obtaining graphene," 2013.

[69] S. Perumal, R. Atchudan, and I. W. Cheong, "Recent studies on dispersion of graphene–polymer composites," *Polymers*, vol. 13, no. 14, p. 2375, 2021.

[70] Qsonica Sonicators, 53 Church Hill Rd, Newtown, CT 06470, *Direct and indirect sonication methods*. Instrument Manual.

[71] W. C. Lai and R. W. Fan, "A simple low-cost method to prepare gel electrolytes incorporating graphene oxide with increased ionic conductivity and electrochemical stability," *Journal of Electroanalytical Chemistry*, vol. 907, p. 115889, 2022.

[72] G. Qi, C. Liang, R. Bao, Z. Liu, W. Yang, B. Xie, and M. Yang, "Polyethylene glycol based shape-stabilized phase change material for thermal energy storage with ultra-low content of graphene oxide," *Solar energy materials and solar cells*, vol. 123, pp. 171–177, 2014.

[73] S. Cheng, D. M. Smith, and C. Y. Li, "Anisotropic ion transport in a poly (ethylene oxide)–liclo4 solid state electrolyte templated by graphene oxide," *Macromolecules*, vol. 48, no. 13, pp. 4503–4510, 2015.

[74] A. Javaid, M. B. Zafrullah, F. H. Khan, and G. M. Bhatti, "Improving the multifunctionality of structural supercapacitors by interleaving graphene nanoplatelets between carbon fibers and solid polymer electrolyte," *Journal of Composite Materials*, vol. 53, no. 10, pp. 1401–1409, 2019.

[75] A. Surnova, D. Balkaev, D. Musin, R. Amirov, and A. M. Dimiev, "Fully exfoliated graphene oxide accelerates epoxy resin curing, and results in dramatic improvement of the polymer mechanical properties," *Composites Part B: Engineering*, vol. 162, pp. 685–691, 2019.

[76] C. Mellado, T. Figueroa, R. Baez, M. Meléndrez, and K. Fernández, "Effects of probe and bath ultrasonic treatments on graphene oxide structure," *Materials Today Chemistry*, vol. 13, pp. 1–7, 2019.

[77] G. T. Le, N. Chanlek, J. Manyam, P. Opaprakasit, N. Grisdanurak, and P. Sreearunothai, "Insight into the ultrasonication of graphene oxide with strong changes in its properties and performance for adsorption applications," *Chemical Engineering Journal*, vol. 373, pp. 1212–1222, 2019.

[78] A. Yasmin, J. Luo, and I. M. Daniel, "Processing of expanded graphite reinforced polymer nanocomposites," *Composites Science and Technology*, vol. 66, no. 9, pp. 1182–1189, 2006.

[79] S. Kumar, A. Garg, and A. Chowdhuri, "Sonication effect on graphene oxide (go) membranes for water purification applications," *Materials Research Express*, vol. 6, no. 8, p. 085620, 2019.

[80] K. Mukhopadhyay, C. D. Dwivedi, and G. N. Mathur, "Conversion of carbon nanotubes to carbon nanofibers by sonication," *Carbon*, vol. 40, no. 8, pp. 1373–1376, 2002.

[81] B. Fiedler, F. H. Gojny, M. H. Wichmann, M. C. Nolte, and K. Schulte, "Fundamental aspects of nano-reinforced composites," *Composites science and technology*, vol. 66, no. 16, pp. 3115–3125, 2006.

[82] T. R. Shah, H. Koten, and H. M. Ali, "Performance effecting parameters of hybrid nanofluids," in *Hybrid Nanofluids for Convection Heat Transfer*, pp. 179–213, Elsevier, 2020.

[83] G. Seretis, I. Theodorakopoulos, D. Manolakos, and C. Provatidis, "Effect of sonication on the mechanical response of graphene nanoplatelets/glass fabric/epoxy laminated nanocomposites," *Composites Part B: Engineering*, vol. 147, pp. 33–41, 2018.

[84] J. Wang, R. Zheng, J. Gao, and G. Chen, "Heat conduction mechanisms in nanofluids and suspensions," *Nano Today*, vol. 7, no. 2, pp. 124–136, 2012.

[85] B. Jóźwiak, H. F. Greer, G. Dzido, A. Kolanowska, R. Jedrysiak, J. Dziadosz, M. Dzida, and S. Boncel, "Effect of ultrasonication time on microstructure, thermal conductivity, and viscosity of ionanofluids with originally ultra-long multi-walled carbon nanotubes," *Ultrasonics Sonochemistry*, vol. 77, p. 105681, 2021.

[86] A. Amrollahi, A. Hamidi, and A. Rashidi, "The effects of temperature, volume fraction and vibration time on the thermo-physical properties of a carbon nanotube suspension (carbon nanofluid)," *Nanotechnology*, vol. 19, no. 31, p. 315701, 2008.

[87] A. Asadi, I. M. Alarifi, V. Ali, and H. M. Nguyen, "An experimental investigation on the effects of ultrasonication time on stability and thermal conductivity of mwcnt-water nanofluid: Finding the optimum ultrasonication time," *Ultrasonics sonochemistry*, vol. 58, p. 104639, 2019.

[88] S. Nam, C. Jung, H. Li, M. Yu, J. R. Flora, L. K. Boateng, N. Her, K. Zoh, and Y. Yoon, "Adsorption characteristics of diclofenac and sulfamethoxazole to graphene oxide in aqueous solution," *Chemosphere*, vol. 136, pp. 20–26, 2015.

[89] J. Chen, M. Duan, and G. Chen, "Continuous mechanical exfoliation of graphene sheets via three-roll mill," *Journal of Materials Chemistry*, vol. 22, no. 37, pp. 19625–19628, 2012.

[90] Y. Li, H. Zhang, E. Bilotti, and T. Peijs, "Optimization of three-roll mill parameters for in-situ exfoliation of graphene," *MRS advances*, vol. 1, no. 19, pp. 1389–1394, 2016.

[91] A. Yasmin, J. L. Abot, and I. M. Daniel, "Processing of clay/epoxy nanocomposites by shear mixing," *Scripta materialia*, vol. 49, no. 1, pp. 81–86, 2003.

[92] M. Raza, A. Westwood, A. Brown, and C. Stirling, "Texture, transport and mechanical properties of graphite nanoplatelet/silicone composites produced by three roll mill," *Composites science and technology*, vol. 72, no. 3, pp. 467–475, 2012.

[93] Y. Li, H. Zhang, M. Crespo, H. Porwal, O. Picot, G. Santagiuliana, Z. Huang, E. Barbieri, N. M. Pugno, T. Peijs, *et al.*, "In situ exfoliation of graphene in epoxy resins: a facile strategy to efficient and large scale graphene nanocomposites," *ACS applied materials & interfaces*, vol. 8, no. 36, pp. 24112–24122, 2016.

[94] J. Ha, S. Lee, and S. Park, "Effect of dispersion by three-roll milling on electrical properties and filler length of carbon nanotube composites," *Materials*, vol. 12, no. 23, p. 3823, 2019.

[95] V. A. Agubra, P. S. Owuor, and M. V. Hosur, "Influence of nanoclay dispersion methods on the mechanical behavior of e-glass/epoxy nanocomposites," *Nanomaterials*, vol. 3, no. 3, pp. 550–563, 2013.

[96] L. Wang, Y. Cui, B. Li, S. Yang, R. Li, Z. Liu, R. Vajtai, and W. Fei, "High apparent strengthening efficiency for reduced graphene oxide in copper matrix composites produced by molecule-lever mixing and high-shear mixing," *RSC Advances*, vol. 5, no. 63, pp. 51193–51200, 2015.

[97] K. R. Paton, E. Varrla, C. Backes, R. J. Smith, U. Khan, A. O'Neill, C. Boland, M. Lotya, O. M. Istrate, P. King, *et al.*, "Scalable production of large quantities of defect-free few-layer graphene by shear exfoliation in liquids," *Nature materials*, vol. 13, no. 6, pp. 624–630, 2014.

[98] E. Pullicino, W. Zou, M. Gresil, and C. Soutis, "The effect of shear mixing speed and time on the mechanical properties of gnp/epoxy composites," *Applied Composite Materials*, vol. 24, no. 2, pp. 301–311, 2017.

[99] Y. Yuan, Z. Liu, B. Wei, Z. Yang, L. Wang, and W. Fei, "Effects of high-shear mixing and the graphene oxide weight fraction on the electrochemical properties of the go/ni (oh) 2 electrode," *Dalton Transactions*, vol. 49, no. 6, pp. 1752–1764, 2020.

[100] M. S. Khan, A. Shakoor, G. T. Khan, S. Sultana, and A. Zia, "A study of stable graphene oxide dispersions in various solvents.," *Journal of the Chemical Society of Pakistan*, vol. 37, no. 1, 2015.

[101] J. Paredes, S. Villar-Rodil, A. Martinez-Alonso, and J. M. Tascon, "Graphene oxide dispersions in organic solvents," *Langmuir*, vol. 24, no. 19, pp. 10560–10564, 2008.

[102] D. Zhu, Y. Bin, and M. Matsuo, "Electrical conducting behaviors in polymeric composites with carbonaceous fillers," *Journal of Polymer Science Part B: Polymer Physics*, vol. 45, no. 9, pp. 1037–1044, 2007.

[103] J. Y. Yi and G. M. Choi, "Percolation behavior of conductor-insulator composites with varying aspect ratio of conductive fiber," *Journal of electroceramics*, vol. 3, no. 4, pp. 361–369, 1999.

[104] C. Berthier, W. Gorecki, M. Minier, M. Armand, J. Chabagno, and P. Rigaud, "Microscopic investigation of ionic conductivity in alkali metal salts-poly(ethylene oxide) adducts," *Solid State Ionics*, vol. 11, no. 1, pp. 91–95, 1983.

[105] M. S. Khan and A. Shakoor, "Ionic conductance, thermal and morphological behavior of peo-graphene oxide-salts composites," *Journal of Chemistry*, vol. 2015, 2015.

[106] T. Sreeprasad and V. Berry, "How do the electrical properties of graphene change with its functionalization?," *small*, vol. 9, no. 3, pp. 341–350, 2013.

[107] J. Hughes, "The carbon fibre/epoxy interface—a review," *Composites Science and Technology*, vol. 41, no. 1, pp. 13–45, 1991.

[108] M. Guigon and E. Klinklin, "The interface and interphase in carbon fibre-reinforced composites," *Composites*, vol. 25, no. 7, pp. 534–539, 1994.

[109] R. Sager, P. Klein, D. Lagoudas, Q. Zhang, J. Liu, L. Dai, and J. Baur, "Effect of carbon nanotubes on the interfacial shear strength of t650 carbon fiber in an epoxy matrix," *Composites Science and Technology*, vol. 69, no. 7-8, pp. 898–904, 2009.

[110] J. Moosburger-Will, J. Jäger, J. Strauch, M. Bauer, S. Strobl, F. F. Linscheid, and S. Horn, "Interphase formation and fiber matrix adhesion in carbon fiber reinforced epoxy resin: influence of carbon fiber surface chemistry," *Composite Interfaces*, vol. 24, no. 7, pp. 691–710, 2017.

[111] J. P. Johnston, B. Koo, N. Subramanian, and A. Chattopadhyay, "Modeling the molecular structure of the carbon fiber/polymer interphase for multiscale analysis of composites," *Composites Part B: Engineering*, vol. 111, pp. 27–36, 2017.

[112] H. Zheng, W. Zhang, B. Li, J. Zhu, C. Wang, G. Song, G. Wu, X. Yang, Y. Huang, and L. Ma, "Recent advances of interphases in carbon fiber-reinforced polymer composites: a review," *Composites Part B: Engineering*, p. 109639, 2022.

[113] P. Xu, Y. Yu, Z. Guo, X. Zhang, G. Li, and X. Yang, "Evaluation of composite interfacial properties based on carbon fiber surface chemistry and topography: Nanometer-scale wetting analysis using molecular dynamics simulation," *Composites Science and Technology*, vol. 171, pp. 252–260, 2019.

[114] Q.-H. Qin and J. Ye, *Toughening mechanisms in composite materials*. Elsevier, 2015.

[115] T. Ma, X. Pei, L. Liu, C. Wang, L. Liu, Z. Xu, Y. Jiang, and N. Wu, "Interfacial shear strength of opaque resin/carbon fiber based on mapping from energy dispersive x-ray spectroscopy," *Polymer Composites*, vol. 41, no. 6, pp. 2134–2144, 2020.

[116] S. Feih, K. Wonsyld, D. Minzari, P. Westermann, and H. Lilholt, "Testing procedure for the single fiber fragmentation test," *Risoe National Laboratory, Roskilde, Denmark*, pp. 1–30, 2004.

[117] M. Rich, L. Drzal, D. Hunston, G. Holmes, W. McDonough, *et al.*, "Round robin assessment of the single fiber fragmentation test," in *Procedings of the American Society for Composites 17th Technical Conference*, 2002.

[118] A. Kelly and a. W. Tyson, "Tensile properties of fibre-reinforced metals: copper/tungsten and copper/molybdenum," *Journal of the Mechanics and Physics of Solids*, vol. 13, no. 6, pp. 329–350, 1965.

[119] L. Liu, C. Jia, J. He, F. Zhao, D. Fan, L. Xing, M. Wang, F. Wang, Z. Jiang, and Y. Huang, "Interfacial characterization, control and modification of carbon fiber reinforced polymer composites," *Composites Science and Technology*, vol. 121, pp. 56–72, 2015.

[120] L. Meng, D. Fan, C. Zhang, Z. Jiang, and Y. Huang, "The effect of oxidation treatment with supercritical water/hydrogen peroxide system on intersurface performance for polyacrylonitrile-based carbon fibers," *Applied surface science*, vol. 273, pp. 167–172, 2013.

[121] J. Xie, D. Xin, H. Cao, C. Wang, Y. Zhao, L. Yao, F. Ji, and Y. Qiu, "Improving carbon fiber adhesion to polyimide with atmospheric pressure plasma treatment," *Surface and coatings technology*, vol. 206, no. 2-3, pp. 191–201, 2011.

[122] L. Liu, L. Li, Y. Gao, L. Tang, and Z. Zhang, "Single carbon fiber fracture embedded in an epoxy matrix modified by nanoparticles," *Composites science and technology*, vol. 77, pp. 101–109, 2013.

[123] J. Zhang, D. He, H. Wagner, E. Wiesel, and J. Bai, "Interfacial studies of carbon fiber/epoxy composites using single fiber fragmentation test," *Composite Interfaces*, vol. 20, no. 6, pp. 421–429, 2013.

[124] C. Wang, J. Li, S. Sun, X. Li, F. Zhao, B. Jiang, and Y. Huang, "Electrophoretic deposition of graphene oxide on continuous carbon fibers for reinforcement of both tensile and interfacial strength," *Composites Science and Technology*, vol. 135, pp. 46–53, 2016.

[125] C.-B. Qu, Y. Huang, F. Li, H.-M. Xiao, Y. Liu, Q.-P. Feng, G.-W. Huang, N. Li, and S.-Y. Fu, "Enhanced cryogenic mechanical properties of carbon fiber reinforced epoxy composites by introducing graphene oxide," *Composites Communications*, vol. 22, p. 100480, 2020.

[126] S. Zavareh and G. Samandari, "Polyethylene glycol as an epoxy modifier with extremely high toughening effect: Formation of nanoblend morphology," *Polymer Engineering & Science*, vol. 54, no. 8, pp. 1833–1838, 2014.

[127] Y. Fang, H. Kang, W. Wang, H. Liu, and X. Gao, "Study on polyethylene glycol/epoxy resin composite as a form-stable phase change material," *Energy Conversion and Management*, vol. 51, no. 12, pp. 2757–2761, 2010.

[128] A. Shrivastava, *Introduction to plastics engineering*. William Andrew, 2018.

[129] H. Yao, X. Sui, Z. Zhao, Z. Xu, L. Chen, H. Deng, Y. Liu, and X. Qian, "Optimization of interfacial microstructure and mechanical properties of carbon fiber/epoxy composites via carbon nanotube sizing," *Applied Surface Science*, vol. 347, pp. 583–590, 2015.

[130] M. S. Mohannad Hossain, Mohammad Chowdhury, "Tensile and flexural properties of woven carbon/epoxy-xd-cnt nanophased composites," 45th SAMPE Fall Technical Conference and Exhibition, Kansas, October 21-24 2013.

[131] P. He, B. Huang, L. Liu, Q. Huang, and T. Chen, "Preparation of multiscale graphene oxide-carbon fabric and its effect on mechanical properties of hierarchical epoxy resin composite," *Polymer Composites*, vol. 37, no. 5, pp. 1515–1522, 2016.

[132] E. Selver, "Tensile and flexural properties of glass and carbon fibre composites reinforced with silica nanoparticles and polyethylene glycol," *Journal of Industrial Textiles*, vol. 49, no. 6, pp. 809–832, 2020.

[133] G. Pramudi, W. W. Raharjo, and D. Ariawan, "Investigation of the flexural and impact strength of recycled carbon fiber (rcf) i polyester composite," in *AIP Conference Proceedings*, vol. 2391, p. 070005, AIP Publishing LLC, 2022.

[134] N. S. Hudak, A. D. Schlichting, and K. Eisenbeiser, "Structural supercapacitors with enhanced performance using carbon nanotubes and polyaniline," *Journal of The Electrochemical Society*, vol. 164, no. 4, p. A691, 2017.

[135] T. Brocks, M. O. H. Cioffi, and H. J. C. Voorwald, "Effect of fiber surface on flexural strength in carbon fabric reinforced epoxy composites," *Applied surface science*, vol. 274, pp. 210–216, 2013.

[136] A. Ávila, L. d. O. Peixoto, A. Silva Neto, J. d. Ávila Junior, and M. Carvalho, "Bending investigation on carbon fiber/epoxy composites nano-modified by graphene," *Journal of the Brazilian Society of Mechanical Sciences and Engineering*, vol. 34, pp. 269–275, 2012.

[137] M. Kim, K. Rhee, J. Lee, D. Hui, and A. K. Lau, "Property enhancement of a carbon fiber/epoxy composite by using carbon nanotubes," *Composites Part B: Engineering*, vol. 42, no. 5, pp. 1257–1261, 2011.

[138] X. Zheng, X. Zhou, L. Zou, S. Hong, L. Yao, and Y. Qiu, "Evaluating the interfacial properties of wrinkled graphene fiber through single-fiber fragmentation tests," *Journal of Materials Science*, vol. 55, no. 3, pp. 1023–1034, 2020.

[139] B. A. Heckert, *POSS-based carbon fiber treatment for enhanced strength and toughness of composites*. PhD thesis, Oklahoma State University, Stillwater, Oklahoma, US, 2021.

[140] ASTM-C1557, "Standard test method for tensile strength and young's modulus of fibers," tech. rep., ASTM International, PA, US, 2020.

[141] ASTM-D790, "Standard test methods for flexural properties of unreinforced and reinforced plastics and electrical insulating materials," tech. rep., ASTM International, PA, US, 2010.

[142] R. R. Teja, "Effect of low constant direct currents on quasi-static mechanical response of carbon fiber polymer matrix composites," Master's thesis, Oklahoma State University, Stillwater, Oklahoma, US, 2018.

[143] A. P. Mouritz, *Introduction to aerospace materials*. Elsevier, 2012.

[144] D. Li, Y. Jiang, S. Lv, X. Liu, J. Gu, Q. Chen, and Y. Zhang, "Preparation of plasticized poly (lactic acid) and its influence on the properties of composite materials," *PLoS One*, vol. 13, no. 3, p. e0193520, 2018.

[145] M. Jouyandeh, Z. Karami, J. A. Ali, I. Karimzadeh, M. Aghazadeh, F. Laoutid, H. Vahabi, M. R. Saeb, M. R. Ganjali, and P. Dubois, "Curing epoxy with polyethylene glycol (peg) surface-functionalized nixfe3-xo4magnetic nanoparticles," *Progress in Organic Coatings*, vol. 136, p. 105250, 2019.

[146] M. Naebe, J. Wang, A. Amini, H. Khayyam, N. Hameed, L. H. Li, Y. Chen, and B. Fox, "Mechanical property and structure of covalent functionalised graphene/epoxy nanocomposites," *Scientific reports*, vol. 4, no. 1, pp. 1–7, 2014.

VITA

Deviprakash Jyothishmathi

Candidate for the Degree of

Master of Science

Thesis: A STUDY ON ELECTRICAL DEGRADATION, PROCESSING AND INTERFACIAL STRENGTH OF CARBON FIBER EPOXY COMPOSITES WITH POLYMERS AND FILLERS

Major Field: Mechanical and Aerospace Engineering

Biographical:

Education:

Completed the requirements for the Master of Science in Mechanical and Aerospace Engineering at Oklahoma State University, Stillwater, Oklahoma in December, 2022.

Completed the requirements for the Master of Science in Mechanical Engineering at Khalifa University, Abu Dhabi, UAE in 2017.

Completed the requirements for the Bachelor of Technology in Mechanical Engineering at Kerala University, Trivandrum, India in 2013.

Professional Memberships:

Tau Beta Pi Engineering Honor Society